

國立臺灣大學電機資訊學院光電工程學研究所

碩士論文

**Graduate Institute of Photonics and Optoelectronics**

**College of Electrical Engineering and Computer**

**Science**

**National Taiwan University**

**Master Thesis**

使用三維追蹤倍頻顯微鏡系統診斷日光角化症

**Application of a Three-dimensional Tracking System**

**with Harmonic Generation Microscope for**

**Diagnosing Multiple Actinic Keratosis**

潘益

**Yi Pan**

指導教授：孫啟光 博士

**Advisor: Chi-Kuang Sun, Ph.D**

**2019. 4**

**Apr. 2019**

---

## 致謝



這篇碩士論文記錄了我在台大近兩年半來的研究生涯，僅希望自己在這方面的研究能為後來的學弟學妹提供一點幫助。首先我要感謝指導教授孫啟光老師，無論是在研究方向、研究進展、實驗細節亦或是科學寫作，我都在老師的幫助下獲益匪淺。感謝台大醫院廖怡華醫生在臨床實驗和皮膚科學方面的指導。感謝 Anatoly Ivanov 教授在 Cr:forsterite laser 優化方面的指導。

感謝魏銘良學長、陳蒼元學長、高健庭學長、林冠宏和高浩正學長在 laser 和臨床實驗方面的教學和討論。感謝賴嘉宏和周廷翰的相關討論，很有幸能與你們一起學習相關的課程。感謝陳勝澤和吳沛哲的實驗協助，感謝你們的幫助。感謝 Rebecca 和李敏慈在繁瑣的行政事務方面的協助。感謝易強光電公司相關工程師的協助，順利完成了導光臂。

感謝研究計劃（MOST 107-2321-B-002-006 和 MOST 106-2221-E-002-156-MY3）的經費資助。

最後我特別感謝我的父母以及女友冉冉，能讓我心無旁騖的研究，完成學業。謝謝你們！

潘益 2019.4.22

---

## 摘要



日光角化症 (AK) 是一種常見的由太陽光引起的皮膚病變。它通常會導致皮膚角質細胞增殖病變。日光角化症的治療非常重要。因為它是浸入式鱗狀細胞皮膚癌 (SCC) 的癌前病變徵兆。而且，隨著年齡的增大，人們患上日光角化症的機率會越來越高。日光角化症患者通常會有多個病灶區域。為了日光角化症精確地診斷，本文提出了使用倍頻顯微鏡系統 (HGM) 作為成像研究工具。倍頻顯微鏡系統提供次微米級別的分辨率，這對於組織病理學檢查是至關重要的。而且倍頻顯微鏡對生物組織造成很小的光學損傷。通過比較倍頻顯微鏡和傳統切片的影像，本論文旨在尋找它們細胞形態學上的一致性，來說明倍頻顯微鏡影像從某種程度上可以代替傳統的切片影像進行診斷。5 名年齡在 70 至 93 歲之間的日光角化症亞洲志願者 (2 名女性和 3 名男性) 參與了這項研究。它含有 1 個離體樣品影像和 4 個活體影像。為了更好地進行臨床試驗，本文還發展了帶導光臂的可移動倍頻影像系統。在本文結果中，倍頻影像和傳統切片圖像均顯示角質層 (SC) 角化不全和角化過度現象。在棘層 (SS) 中，顯示不規則棘皮症，棘層結構異常，棘層細胞和細胞核的多形現象。在基底層 (SB) 中，均顯示基底細胞擁擠，細胞形態結構異常。在真皮中，倍頻影像還可以看出膠原蛋白組織日光彈性性變。此外，本文還說明了在倍頻圖像中發現的樹突狀結構細胞。本文的案例研究顯示，倍頻顯微影像有潛力成為日光角化症診斷的替代方案，也有助於醫師從事術後追蹤。

---

關鍵詞：倍頻顯微術，日光角化症，活體光學切片，細胞組織形

態



---

# ABSTRACT



Actinic keratosis (AK) is a common cutaneous neoplasm consisting of proliferation of atypical epidermal keratinocytes resulting from severe solar damage. AKs are important because of their potential to develop into invasive cutaneous squamous cell carcinoma (SCC) with the highest incidence in the aged population. AK patients usually have multiple AKs. To study the diagnosis of AK, *in vivo* harmonic generation microscopy (HGM) was proposed as the imaging tool. HGM provides submicron resolution crucial for histopathological examination and causes little optical damage in bio-tissues. With HGM, this thesis is aimed at seeking out the consistent cell morphology in comparison with the H&E stained histopathological images. Five Asian volunteers (2 females and 3 males) aged from 70 to 93 years old with AK were enrolled in this study. It contained 1 *ex vivo* and 4 *in vivo* examinations. Due to the clinical demands, we also developed movable HGM system with light guide in this study. HGM and H&E images of AK both show parakeratosis and hyperkeratosis in the stratum corneum (SC), irregular acanthosis, abnormal architecture and pleomorphism of cells and nuclei in the stratum spinosum (SS), crowding of keratinocytes, abnormal architecture and pleomorphism of cells and nuclei in the stratum basale (SB), and solar elastosis in the dermis. Moreover, we also found dendritic-like cells in AK through HGM images. Our case study indicates that noninvasive HGM may become an alternative to invasive biopsy in the diagnosis of AKs and also helps physician to improve follow-up treatment assessment.

---

Key words: harmonic generation microscopy, actinic keratosis, *in vivo* optical biopsy, cell morphology



---

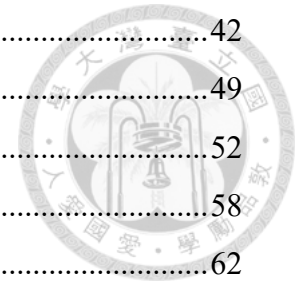
# CONTENTS



致谢.....	i
摘要.....	ii
ABSTRACT.....	iv
CONTENTS.....	vi
LIST OF FIGURES .....	1
LIST OF TABLES .....	11
Chapter 1 Introduction .....	13
1.1 Motivation .....	13
1.2 Thesis Scope.....	15
Chapter 2 Basic Concept.....	16
2.1 Harmonic Generation Microscope .....	16
2.2 Epidermis of Skin.....	18
2.3 Actinic Keratoses .....	19
2.3.1 Clinical Presentation of Actinic Keratoses .....	20
2.3.2 Histopathologic Features of Actinic Keratoses .....	20
2.3.3 Comparing AK and Normal Tissues with H&E Examination .....	22
2.3.4 Treatment.....	24
Chapter 3 Optical Tracking System Setup.....	26
3.1 3D Camera Tracking System .....	26
3.2 Optical System Setup .....	28
3.3 Movable Optical System Setup .....	31
Chapter 4 Materials and Methods .....	36
4.1 Protocol of the Clinical Trial.....	36
4.2 Image Acquisition .....	37
Chapter 5 Results and Discussion.....	39
5.1 Images of the 3D Tracking System .....	39
5.2 Images of HGM.....	40
5.2.1 Normal Epidermal Images of HGM .....	41

---

5.2.2 Result of the AK Patient 00.....	42
5.2.3 Result of the AK Patient 01.....	49
5.2.4 Result of the AK Patients 03 and 04.....	52
5.2.5 Result of the AK Patient 02.....	58
5.2.6 Summary.....	62
5.3 Discussion .....	63
REFERENCES .....	73
COPYRIGHT.....	76





---

# LIST OF FIGURES



**Fig. 2.1.1** (a) Second-harmonic generation process. (b) Energy level in second-harmonic generation. (p17)

**Fig. 2.1.2** (a) Third-harmonic generation process. (b) Energy level in second-harmonic generation. (p17)

**Fig. 2.2.1** (a) A cross-section of all skin layers. (b) A schematic image showing a transverse section of the epidermis, with epidermal layers labeled.[28] Copyright: H. Gray, "Anatomy of the Human Body." in public domain. (p18)

**Fig. 2.3.2.2** (a) Histology (H&E) of AK. (b) Histology (H&E) of normal skin. Scale bar=20  $\mu\text{m}$ . Copyright: J. Lanoue, C. Chen, G. Goldenberg, "Actinic keratosis as a marker of field cancerization in excision specimens of cutaneous malignancies." *Cutis*. 2016, 2016, 97:6 (415-420) with permission from Wolters Kluwer health, Inc. (p22)

**Fig. 2.3.3.1** (a) Histology (H&E) of Bowenoid AK in the stratum corneum: parakeratosis/hyperkeratosis in the arrows. Copyright: own work in Wikimedia commons, Nephron. With permission from owner Nephron. (b) Histology (H&E) of normal skin in the stratum corneum. Scale bar=20  $\mu\text{m}$ . Copyright: A. Day, S. M. Holland, J. P. Scurry, "Normal vulvar histology: variation by site." *Journal of Lower Genital Tract Disease*, 2016, 20:1 (64-69) with permission from Wolters Kluwer health, Inc. (p23)

**Fig. 2.3.3.2** Histology (H&E) of AK. Scale bar=20  $\mu\text{m}$ . It is marked the different situations in the stratum spinosum and the stratum basale. Copyright: J. Lanoue, C.

---

Chen, G. Goldenberg, “Actinic keratosis as a marker of field cancerization in excision specimens of cutaneous malignancies.” *Cutis*. 2016, 2016 ,97:6 (415-420) with permission from Wolters Kluwer health, Inc. **(p23)**

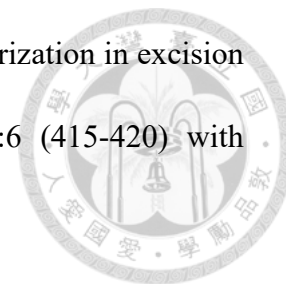


**Fig. 3.1.1** 3D Camera-EinScan-Pro 3D camera. **(p27)**

**Fig. 3.1.2** (a) 3D Camera-EinScan-Pro 3D camera and the calibration plate. (b) The operation window with calibration step 1. Gray plaids need to be lighted on in the red circle. (c) The calibration plate is set obliquely. The camera shoots a purple cross of light to the white area. (d) The purple cross of light in the white area. (within the red circle) (e) The operation window with calibration step 2. Gray plaids need to be lighted on shown as in the red circle. (f) The camera shoots purple lines (in the red circle) of light to the white area. **(p27)**

**Fig. 3.2.1** A schematic diagram of the optical harmonic generation microscopy system used in the clinical trials. DBS: dichroic beam splitter; PMT: photomultiplier tube; BPS: band-pass filter. **(p30)**

**Fig. 3.2.2** The mechanical structure of the optical harmonic generation microscopy system. DBS: dichroic beam splitter; PMT: photomultiplier tube; SHG: second harmonic generation; THG: third harmonic generation. **(p30)**

**Fig. 3.2.3** Photos of the harmonic generation microscopy system. (a) Side view. (b) Front view. (c) Upward front view. **(p30)**

**Fig. 3.3.1** A schematic diagram of the movable optical harmonic generation microscopy system with a light guide. DBS: dichroic beam splitter; PMT: photomultiplier tube; BPS: band-pass filter. **(p31)**

---

**Fig. 3.3.2** (a) The mechanical structure of the optical harmonic generation microscopy system. Light guide and anti-gravity arm are integrated with an image head. (b) The detailed mechanical structure of the image head. DBS: dichroic beam splitter; PMT: photomultiplier tube; SHG: second harmonic generation; THG: third harmonic generation. (p32)

**Fig. 3.3.3** The whole system in reality. (a) Down view. (b) Side view. (c) Front view. (d) Image head. (p32)

**Fig. 3.3.4** (a) The sketch of alignment with duma. (b) Two adjustment screw pairs in the circles 1 and 2 in a part of light guide. (c) A small cross drawing a semicircle on the screen. (p35)

**Fig. 4.1.2** The protocol of the whole clinical trial. (p36)

**Fig. 4.2.1** (a) The illustration on how a plastic ring was used to prevent acquiring images outside the lesion. (b) The electric hospital bed with a volunteer. (p38)

**Fig. 5.1.1** 3D camera images of AK 01 patient's lesion. (a) AK lesion area is  $4.835 \text{ cm}^2$ . (Location in yellow marked.) (b) The length of AK lesion is 2.351 cm. (c) The width of AK lesion is 0.861 cm. (p39)

**Fig. 5.1.2** 3D camera images of AK 02 patient's lesion. (a) The location and clinical presentation of the AK lesion before treatment (red circle). (b) The location and clinical presentation of the AK lesion 2 months after treatment (red circle). (c) The location and clinical presentation of the AK lesion 4 months after treatment (red circle). (p39)

---

**Fig. 5.1.3** (a) 3D camera images of AK 03 patient's lesion. The location of AK is marked with a red arrow. (b) 3D camera images of AK 04 patient's lesion. The location of AK is marked with a red arrow. (p40)

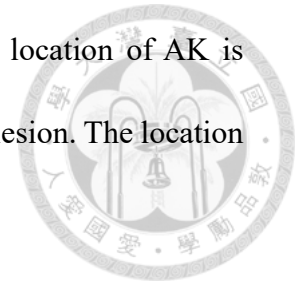


**Fig. 5.2.1** [(a) to (f)] A representative series of *in vivo* HGM images at different depths relative to the surface (5.4, 14.4, 30.6, 52.2, 75.6 and 111.6  $\mu\text{m}$ ). (a) Stratum corneum. (b) Stratum granulosum. (c) Stratum spinosum. (d) and (e) Stratum basale. (f) Dermis. Scale bar=50  $\mu\text{m}$ . (p43)

**Fig. 5.2.2.1** A transverse histopathology section of the AK patient 00 on the skull. Lines a, b, c, d, e and f represent depths in the epidermis corresponding to *en face* sections in Fig. 5.2.2.2. Line a is in the stratum corneum. Line b is in the stratum granulosum. Lines c and d are in the stratum spinosum. Line e is in the stratum basale and line f is in the dermis. Scale bar=10  $\mu\text{m}$ . (p43)

**Fig. 5.2.2.2** Actinic keratoses [(a) to (f)] A representative series of *ex vivo* HGM *en face* sectioned images at different depths relative to the surface (24, 90, 127, 199, 233 and 248  $\mu\text{m}$ ) in AK patient 00. The lesion is on the skull. (a) Stratum corneum. There are nuclei (black hole) in the red arrow. (b) Stratum granulosum. (c) and (d) Stratum spinosum. (e) Stratum basale. (f) Dermis. Scale bar=50  $\mu\text{m}$ . (p43)

**Fig. 5.2.2.3** A transverse histopathology section of the AK patient 00 on the skull. (a) Stratum corneum. Parakeratosis and hyperkeratosis are obvious to see. The thickness of the stratum corneum is thicker than normal one. (b) Stratum granulosum and stratum spinosum. These cells are all in different sizes and abnormal architecture. Irregular acanthosis is noted in the stratum spinosum. In the circle 1, the pleomorphism of nuclei

---

is in the cell and cells are in different sizes. In the circle 2, the cell loses polarity and they are irregular acanthosis. (c) Stratum basale. Abnormal architecture is in the stratum basale. The cells are in different sizes and shapes crowding to each other. In the circle 1, the basal cells are slender and bending not like the normal ellipse. In the circle 2, cells are in pleomorphism. In the circle 3, cells are crowding to each other and in different sizes. Scale bar=10  $\mu\text{m}$ . (p43)

**Fig. 5.2.2.4** The noise HGM image of the normal volunteer. Scale bar=50  $\mu\text{m}$ . (p46)

**Fig. 5.2.2.5** THG images and its pixel intensity changing. (a) The HGM image of normal connective tissues without SHG signal in normal volunteer. (b) The pixel intensity of THG signal of normal connective tissues in image(a). (c) The connective tissue of HGM image of AK patient 00 without SHG signal. (d) The pixel intensity of THG signal of AK patient 00's connective tissues in image (c). Scale bar=50  $\mu\text{m}$ . (p48)

**Fig. 5.2.2.7** The transverse sectioned images of the stratum basale of AK patient 00 in the same left cheek lesion. (a) The labeled image is HGM of AK. (b) The labeled image is the conventional histopathology of AK. In the red circle (a), the black hole representing the nuclei of the basal cell takes up the majority of the cell volume. In the red circle (b), the darker hole representing the nuclei of the basal cell takes up the majority of the cell volume. In the red arrows, cells are crowding to each other. In the green arrows, these cells are bending and slender. Scale bar=10  $\mu\text{m}$ . (p47)

**Fig. 5.2.3.1** A transverse histopathology section of the AK patient 01 on the skull. In the stratum corneum, it shows hyperkeratosis. In the stratum basale, it shows

---

architectural disarray, crowding keratinocytes and cytologic atypia with large and pleomorphic nuclei and cells (red circle). Scale bar=10  $\mu\text{m}$ . (p49)

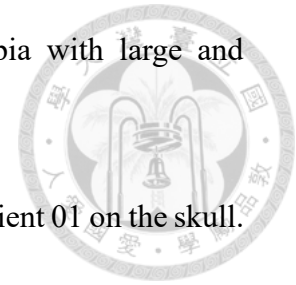


**Fig. 5.2.3.2** *In vivo* HGM *en face* virtual sectioned images of AK patient 01 on the skull.

[(a) to (c)] A representative series of *in vivo* HGM images taken at different depths relative to the surface in AK patient 01. (a) Stratum corneum. (b) Stratum basale. (c) Stratum basale. In the red circles (b) and (c), it shows that nuclei take up the majority of the cell volume. Scale bar=50  $\mu\text{m}$ . (p50)

**Fig. 5.2.4.1** Two transverse histopathology sections of the AK patient 03 in the same lesion of cheek. (a) In the stratum corneum, hyperkeratosis is obvious to see and there is no parakeratosis. The thickness of the stratum corneum is thicker than the normal one. In the stratum spinosum, cell atypia is not obvious to see and it shows normal architecture. Irregular acanthosis exists in the stratum spinosum. In the stratum basale, abnormal architecture is obvious. The cells crowding to each other are in different sizes and shapes. In the circle 1, solar elastosis happens in the dermis. The connective tissues change into purple while the normal connective tissues are pink in H&E image. In the circle 2, the basal cells are pigmented. (b) In the red circle, cell atypia is obvious in the stratum spinosum. Scale bar=10  $\mu\text{m}$ . (p52)

**Fig. 5.2.4.2** Actinic keratosis [(a) to (d)] A representative series of *in vivo* HGM *en face* sectioned images at different depths relative to the surface in AK patient 03. The lesion is on the cheek. (a) Stratum corneum. There is hyperkeratosis and not parakeratosis. (b) Stratum spinosum. Stratum spinosum shows architectural disarray and cytologic atypia with large and pleomorphic nuclei and cells in the red circle. (c) Stratum basale. The

---

stratum basale shows architectural disarray, crowding keratinocytes and cytologic atypia with large and pleomorphic nuclei and cells. (d) Dermis. Scale bar=50  $\mu\text{m}$ . (p52)

**Fig. 5.2.4.3** A transverse histopathology section of the AK patient 04 on the cheek. In the stratum corneum, hyperkeratosis is obvious to see and there is parakeratosis in label. The thickness of the stratum corneum is thicker than the normal one. In the stratum spinosum, these cells are all in different sizes and it indicted abnormal architecture. Irregular acanthosis is in the stratum spinosum. In the stratum basale, abnormal architecture is obvious. The cells crowding to each other are in different sizes and shapes. In the circle 1, connective tissues are normal and pink. In the circle 2, solar elastosis happens in the dermis. The connective tissues change into purple amorphous appearance. Scale bar=10  $\mu\text{m}$ . (p53)

**Fig. 5.2.4.4** Actinic keratosis [(a) to (c)] A representative series of *in vivo* HGM *en face* sectioned images at different depths relative to the surface in AK patient 04. The lesion is on the cheek. (a) Stratum spinosum. Stratum spinosum shows architectural disarray and cytologic atypia with large and pleomorphic nuclei and cells in the red circles. (b) Stratum basale. The stratum basale shows architectural disarray, crowding keratinocytes and cytologic atypia with large and pleomorphic nuclei and cells. (c) Dermis. Scale bar=50  $\mu\text{m}$ . (p54)

**Fig. 5.2.4.5** THG images without SHG signal and its pixel intensity changing. (a) The THG image of normal connective tissue without SHG signal in normal volunteer. (b) The pixel intensity of THG signal of normal connective tissue in the image (a). (c) The connective tissue of THG image of AK patient 03 without SHG signal. (d) The pixel

---

intensity of THG signal of AK patient 03's connective tissue in image(c). (e) The connective tissue of THG image of AK patient 04 without SHG signal. (f) The pixel intensity of THG signal of AK patient 04's connective tissue in the image (e). Scale bar=50  $\mu\text{m}$ . (p56)

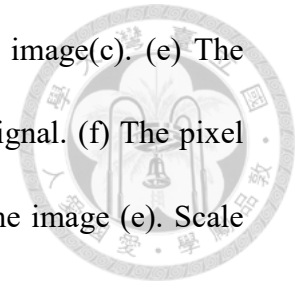


**Fig. 5.2.5.1** A transverse histopathology section of the AK patient 02 on the cheek. In the stratum corneum, it is normal. In the stratum spinosum, it is normal as well. In the stratum basale, the cells crowding to each other are in different sizes and shapes in the circle 1. In the circle 2, basal cells are normal. Scale bar=10  $\mu\text{m}$ . (p58)

**Fig. 5.2.5.2** Actinic keratosis [(a) and (b)] A representative series of *in vivo* HGM *en face* sectioned images at different depths relative to the surface in AK patient 02. The lesion is on the cheek. (a) Stratum spinosum. The stratum spinosum is normal. (b) Stratum basale. The stratum basale shows crowding keratinocytes and cytologic atypia with pleomorphic cells in the circle 1. In the circle 2, the basal cells are normal. Scale bar=50 $\mu\text{m}$ . (p59)

**Fig. 5.2.5.3** THG images without SHG signal and its pixel intensity changing. (a) The HGM image of normal connective tissue without SHG signal in normal volunteer. (b) The pixel intensity of THG signal of normal connective tissue in image(a). (c) The connective tissue of HGM image of AK patient 02 without SHG signal. (d) The pixel intensity of THG signal of AK patient 02's connective tissue in image(c). Scale bar=50  $\mu\text{m}$ . (p59)

**Fig. 5.2.5.5** *En face* sectioned HGM images of AK patient 02 in the same location after two months. [(a) to (c)] The lesion is on the cheek. (a) Stratum corneum. It is normal.



---

(b) Stratum spinosum. It is normal. (c) Stratum basale. It is normal. Scale bar=50  $\mu\text{m}$ .

(p61)

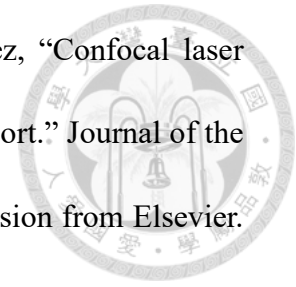
**Fig. 5.3.1** *En face* sectioned *ex vivo* and *in vivo* HGM images of AK patients in the stratum basale. (a) The stratum basale of AK patient 00. In the red circle, it shows dendritic-cell-like signals. (b) The stratum basale of AK patient 01. In the red circle, it is dendritic-cell-like signals. (c) The stratum basale of AK patient 03. In the red circle, it is dendritic-cell-like signals. (a) The stratum basale of AK patient 04. In the red circle, it is dendritic-cell-like signals. (p63)

**Fig. 5.3.3** Example of OCT-images presented in the study set. (A) Normal skin located on the arm, showing a narrow, hyperreflective band corresponding to an entry signal (thick arrow). The epidermis is seen as a homogenous well-demarcated darker layer (marked by \*). The dermis is seen as a lighter layer (marked by \*\*) and the DEJ is seen as a clear transition between the layers (thin arrow). (C) AK lesion located on the scalp, showing thickening of the epidermis (marked by \*) and purple streaks in the upper epidermis due to hyperkeratosis (thick arrow). The DEJ is disrupted beneath the thickened epidermis (marked by \*\*). Copyright: J. Olsen, L. Themstrup, N. De Carvalho, M. Mogensen, G. Pellacani, G. B. E. Jemec, "Diagnostic accuracy of optical coherence tomography in actinic keratosis and basal cell carcinoma", *Photodiagnosis and Photodynamic Therapy*, 2016, 16 (44-49) with permission from Elsevier. (p65)

**Fig. 5.3.4** Horizontal sections from depths in epidermis. Left column is conventional histopathology of AK, center is RCM of AK, and right column is RCM of adjacent normal skin. (A) Stratum corneum. (B) Stratum granulosum. (C) Stratum spinosum. (D)

---

Stratum basale. Copyright: D. Aghassi, R. Anderson, S. González, “Confocal laser microscopic imaging of actinic keratoses *in vivo*: A preliminary report.” Journal of the American Academy of Dermatology, 2000, 43 (42-48) with permission from Elsevier.



**(p66)**

**Fig. 5.3.5** The stratum corneum (A–C) RCM images; (D–F) representative histologic images. Copyright: M. Mlrich, A. Maltusch, F.-D. Rius, J. Röwert-Huber, S. González, W. Sterry, E. Stockfleth, S. Astner, “Clinical applicability of *in vivo* reflectance confocal microscopy for the diagnosis of actinic keratoses.” Dermatologic Surgery, 2008, 34:5 (610-619) with permission from Elsevier. **(p67)**

**Fig. 5.3.6** Stratum granulosum and stratum spinosum (A–C) RCM images; (D–F) representative histologic images. Copyright: M. Mlrich, A. Maltusch, F.-D. Rius, J. Röwert-Huber, S. González, W. Sterry, E. Stockfleth, S. Astner, “Clinical applicability of *in vivo* reflectance confocal microscopy for the diagnosis of actinic keratoses.” Dermatologic Surgery, 2008, 34:5 (610-619) with permission from Elsevier. **(p67)**

**Fig. 5.3.7** Dermis (A, B) RCM images; (C, D) representative histologic images. Copyright: M. Mlrich, A. Maltusch, F.-D. Rius, J. Röwert-Huber, S. González, W. Sterry, E. Stockfleth, S. Astner, “Clinical applicability of *in vivo* reflectance confocal microscopy for the diagnosis of actinic keratoses.” Dermatologic Surgery, 2008, 34:5 (610-619) with permission from Elsevier. **(p67)**

---

# LIST OF TABLES



**Table 2.3.2.1** Histopathologic feature of AK for diagnosis criterion of HGM images.

(p22)

**Table 4.1.1** Information of every volunteers. (p36)

**Table 5.2.2.5** The evaluation results of H&E and HGM for AK patient 00. “+” represents that this feature can be recognized. “-” represents that this feature does not exist. “NA” represents that this feature is uncertain to recognize. (p47)

**Table 5.2.3.3** The evaluation results of H&E and HGM for AK patient 01. “+” represents that this feature can be recognized. “-” represents that this feature does not exist. “NA” represents that this feature is uncertain to recognize. (p51)

**Table 5.2.4.6** The evaluation results of H&E and HGM for AK patient 03 and 04. “+” represents that this feature can be recognized. “-” represents that this feature does not exist. “NA” represents that this feature is uncertain to recognize. (p57)

**Table 5.2.4.4** The evaluation results of H&E and HGM for AK patient 02. “+” represents that this feature can be recognized. “-” represents that this feature does not exist. “NA” represents that this feature is uncertain to recognize. (p60)

**Table 5.2.6.1** Summary of diagnosis results of 5 patients. “+” represents that this feature can be recognized. “-” represents that this feature does not exist. “NA” represents that this feature is uncertain to recognize. AK grade represents the severity of AK. AK grade III represents serious AK. AK grade II represents middle AK. AK grade I represents mild AK. (p62)

---

**Table 5.3.2** The basal distribution of THG-bright dendritic-cell-like signals in 5 AK patients. “+” represents that this feature can be recognized. “-” represents that this feature does not exist. AK grade represents the severity of AK. AK grade I represents mild AK. AK grade II represents moderate AK. AK grade III represents severe AK.

**(p63)**

**Table 5.3.8** Comparison of OCT, RCM and HGM. **(p69)**

**Table 5.3.9** Diagnosis criterions of HGM, RCM and OCT. “+” represents that this feature can be recognized. “-” represents that this feature is uncertain to recognize. **(p69)**

---

# Chapter 1 Introduction



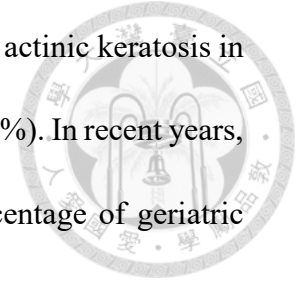
## 1.1 Motivation

Actinic keratosis (AK) is a common cutaneous neoplasm consisting of proliferation of atypical epidermal keratinocytes resulting from severe solar damage.<sup>[1][2]</sup> AKs are clinically important lesions because of their potential to develop into invasive cutaneous squamous cell carcinoma (SCC) with the highest incidence in the aged population.<sup>[3][4]</sup> SCC is a type of skin cancer and sometimes becomes fatal if left untreated. The probability that AK will evolve into SCC was estimated at 0.075-0.096% per lesion per year.<sup>[5]</sup> Therefore, for a person with an average of 7.7 lesions of AK, the incidence of SCC would be 10.2% in 10 years.<sup>[6]</sup> Studies have also concluded more than 200,000 SCC cases each year in America. Approximately 10% of AKs will progress to SCCs.<sup>[7]</sup> What's more, an estimated 1200 persons die of metastatic SCC each year currently.<sup>[8]</sup> In addition to SCC, AK also represents a strong predictor for the development of melanoma or basal cell carcinoma.<sup>[9]</sup> Patients with AKs should be carefully screened for skin malignancy.

AKs are very common with estimated prevalence of 39.5 million in 2004 alone, 26 million of which were patients over 65 years of age all around the world.<sup>[4]</sup> In Taiwan, from a 7-year survey (1993-1999) for geriatric patients in National Taiwan University Hospital, AK is the second most common skin malignancy among 22.4% of the malignant tumor cases.<sup>[10]</sup> Within a total of 16,924 patients aged 65 years and older, cutaneous malignant tumors were found in 2.1%. That means there are about 11 AK

---

NTUH patients each year (Basal cell carcinoma occurred in 29.8%, actinic keratosis in 22.4%, Bowen's disease in 13.3% and squamous cell carcinoma 13.3%). In recent years, there is an increased disease burden of AK in Taiwan as the percentage of geriatric populations increased tremendously.



Most people get more than one AK lesion, and patients who have multiple AKs continue to get new AKs for life. Clinical diagnosis and treatment follow-up for multiple AKs mainly depend on visual inspection and direct counting of all visible lesions. Problems in the direct counting approach may reside in difficulty in dealing with small or almost contiguous lesions. In addition, it is difficult to track the same AK lesion according to the location on the face and its size progression if there are multiple lesions scattered on the whole face. Evaluating treatment efficacy also requires reliable quantification of AKs in the same position before and after treatment. For further research and possibility of automatic diagnosis and care of AKs, standardized and quantized tracking image database should be created.

Exact diagnosis is important to segregate premalignant and malignant lesions prior to treatment. Although histopathology is the gold standard for diagnosis of AK, however, it is not practical to perform invasive skin biopsy for each of the multiple lesions. Histological evaluation is necessarily performed in clinical cases nowadays. To reduce patients' pain based on humanitarian and take care of every AK lesion, it's a pressing need to consider a non-invasive way instead of the traditional biopsy. Nowadays, there are many kinds of non-invasive way to diagnose AKs, such as optical coherence tomography (OCT) and reflectance confocal microscopy (RCM). They have

---

been reported to evaluate the morphological features of AKs and have the potential talent for the diagnosis.<sup>[11][12][13][14]</sup> The image results of these optical imaging modalities left some rooms for improvement due to the relatively poor resolution and contrast. Harmonic generation microscopy (HGM) has been proved to have better performance on *in vivo* human tissue observation with the characteristics of fine contrast, high resolution, deep penetration, and non-invasiveness.<sup>[15][16][17][18]</sup> In this thesis, we have conducted a clinical trial to examine the performance of the HGM on the diagnosis of AK.

## 1.2 Thesis Scope

This thesis is arranged in the following order. Chapter 2 introduces some background knowledge of the thesis, including what is harmonic generation microscope (HGM), basic optical principles of HGM, and what is AK. Chapter 3 details the clinical trial system including a 3D camera tricking system and the optical system we used. Chapter 4 shows the method and protocol of our clinical trials. Finally, in Chapter 5 there are results and discussions. The conclusion and some future prospects are also in Chapter 5.

---

## Chapter 2 Basic Concept



### 2.1 Harmonic Generation Microscope

Harmonic generation microscope (HGM) is a kind of nonlinear microscope with pulsed lasers to generate and drive different nonlinear processes within samples. For biological safety, HGM is guaranteed by its energy conversion mechanism with a high-peak power and low average power pulse laser. The peak power of a single pulse and the average power of laser are expressed as:

$$P_{\text{peak}} = \text{energy per pulse} / \text{pulse duration} \quad (2.1)$$

$$P_{\text{ave}} = \text{energy per pulse} * \text{number of pulses per second} \quad (2.2)$$

where the number of pulses per second is equal to the repetition rate of the laser.

Given the development of the femtosecond pulse laser and nonlinear optical techniques including multi-photon fluorescence<sup>[19]</sup>, second-harmonic generation (SHG)<sup>[20]</sup> and third-harmonic generation (THG)<sup>[21]</sup>, there have produced many new optical microscopes. For our HGM, SHG and THG are both used.

The SHG process can be described as in Fig. 2.1.1. Considering the nonlinearity in the atomic response, an atom under the input light field at an angular frequency  $\omega$  generates new dipole moments at an angular frequency  $2\omega$ . When the relative phases of these dipoles are coherent, the field radiated by each dipole will add as the SHG radiation. Therefore, the SHG process does not involve any real state and it's called a virtual-transition process. Given this, SHG is known with no energy absorption as shown in Fig. 2.1.1(b).



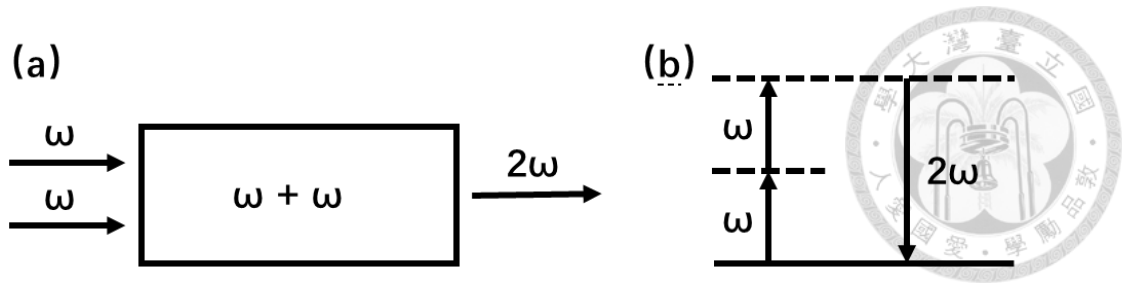


Fig. 2.1.1 (a) Second-harmonic generation process. (b) Energy level in second-harmonic generation.

The THG is a third-order nonlinear optical process. Three photons at angular frequency  $\omega$  are combined as a new photon of angular frequency  $3\omega$  in the nonlinear material as shown in Fig. 2.1.2.

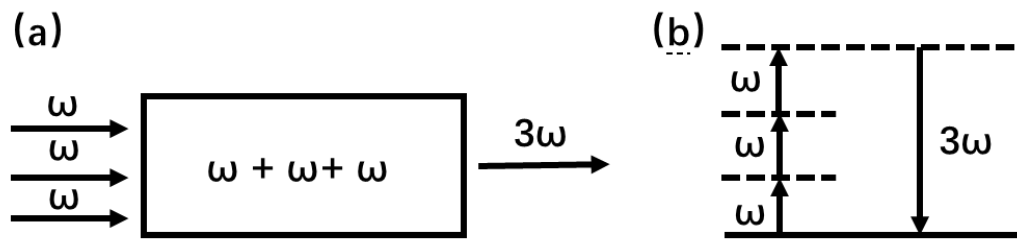


Fig. 2.1.2 (a) Third-harmonic generation process. (b) Energy level in second-harmonic generation.

By the theory of SHG and THG, we can know the resolution of SHG microscope and THG microscope as ('n' is the refractive index related to wavelength ' $\lambda$ '. 'NA' is the numerical aperture of objective.)<sup>[22]</sup>:

$$\text{Lateral resolution of SHG microscope} = 0.43 * n * \lambda / \text{NA} \quad (2.3)$$

$$\text{Axial resolution of SHG microscope} = 0.71 * n * \lambda / \text{NA}^2 \quad (2.4)$$

$$\text{Lateral resolution of THG microscope} = 0.35 * n * \lambda / \text{NA} \quad (2.5)$$

$$\text{Axial resolution of THG microscope} = 0.58 * n * \lambda / \text{NA}^2 \quad (2.6)$$

HGM utilizing SHG and THG is well-developed to have high performance on *in vivo* human tissue observation with the characteristics of high resolution, deep penetration, and non-invasiveness.<sup>[23][24][25]</sup> SHG can provide contrast on materials with no centro symmetry such as collagen fibrils in skin; THG reveals miscellaneous

structures such as cell nucleus and melanin.<sup>[26]</sup> Unlike traditional histological transversal sectioned biopsies, HGM images are *en face* sectioned.



## 2.2 Epidermis of Skin

The epidermis is the outer layer of the three layers that make up the skin, with the inner layers being the dermis and hypodermis, as shown in Fig. 2.2.1.<sup>[27]</sup>

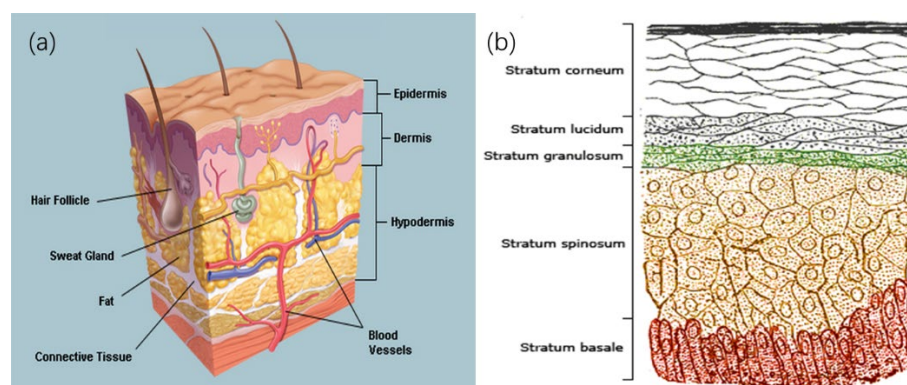
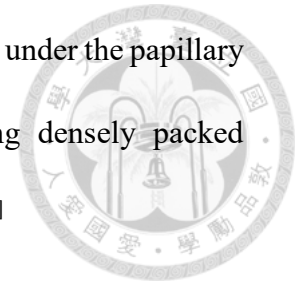


Fig. 2.2.1 (a) A cross-section of all skin layers. (b) A schematic image showing a transverse section of the epidermis, with epidermal layers labeled.<sup>[28]</sup> Copyright: H. Gray, "Anatomy of the Human Body." in public domain.

The epidermis is composed of 4 or 5 sub-layers depending on the region of skin being considered. First sub-layer is the stratum corneum, composed of 10 to 30 layers of polyhedral, enucleated corneocytes. The stratum lucidum presents only in palms and soles. In the stratum granulosum, keratinocytes lose their nuclei and their cytoplasm appears granular. Cells in the stratum spinosum become connected through desmosomes and start produce lamellar bodies. The stratum basale is composed mainly of proliferating and non-proliferating keratinocytes. Below the stratum basale, it's dermis. The papillary dermis is the uppermost layer of the dermis. It intertwines with the rete ridges of the epidermis and is composed of fine and loosely arranged collagen

---

fibers.<sup>[29]</sup> The reticular dermis is the lower layer of the dermis, found under the papillary dermis, composed of dense irregular connective tissue featuring densely packed collagen fibers. It is the primary location of dermal elastic fibers.<sup>[30]</sup>



## 2.3 Actinic Keratoses

Actinic keratoses are proliferations of transformed, neoplastic keratinocytes that are confined to the epidermis and induced by exposure to UV radiation in sunlight. Neoplastic (of or related to or having the properties of a neoplasm, ((腫瘤) 瘤化的) transformation occurs in keratinocytes that have been exposed to UV radiation and is due primarily to mutations in the p53 gene. In times, these cells proliferate in the epidermis and eventually extend into the dermis, at which point metastatic (relating to or affected by metastasis, ((癌細胞的) 轉移性, 變性) spread can occur.<sup>[8]</sup> Cytologic atypia is visible in early stages and is identical to that seen in metastatic lesions or in SCC in the dermis. While these cells remain confined to the epidermis, the lesions that they cause are termed actinic keratoses, but when they extend more deeply to involve the papillary and/or reticular dermis, they are termed SCC. Thus, AK and SCC are rather a progression along a spectrum but not new.<sup>[31]</sup>

---

### 2.3.1 Clinical Presentation of Actinic Keratoses



Actinic keratoses occur on sun-exposed areas such as the face, lower lip, bald scalp, neck, arms, and hands. They appear as rough, scaly papules and plaques that range from skin tone to reddish brown. The papules and plaques range in size from 1 mm to 2.5 cm or more in diameter. Most affected individuals develop multiple lesions. Because AKs develop after years of sun damage, they occur on older patients and increase in number with age. We show clinical images of AKs in chapter 5.1.

The probability that AK would evolve into SCC was estimated at 0.075-0.096% per lesion per year.<sup>[5]</sup> Therefore, for a person with an average of 7.7 lesions of AK, the incidence of SCC would be 10.2% in 10 years.<sup>[6]</sup> Other sources give even higher estimates, with rates of 13% to 20% of all untreated AK lesions of low and moderate grade will progress to SCC *in situ* and invade deeper dermal tissues if left untreated over a 10-year period.<sup>[32][33]</sup>

### 2.3.2 Histopathologic Features of Actinic Keratoses

The diagnosis of AK is usually made on the basis of clinical characteristics while a biopsy may be required to exclude deeper involvement especially when the lesion is large, bleeding, ulcerated, erythematous, indurated, or otherwise unusual. Because many other diseases cause the same symptoms. Several rare histologic variants, including pigmented, acantholytic (皮膚棘層鬆懈的), and hyperplastic (增生性, 肥大的) types, have also been described. All these rare variants share the characteristic

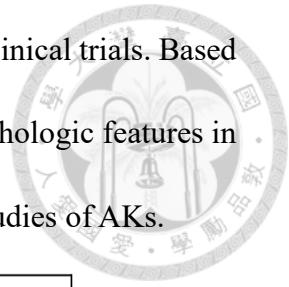
---

of atypical keratinolytic proliferation in the epidermis. For discussion in this thesis, only classical features will be mentioned in the comparison and discussion shown in Table 2.3.2.1. However, we still show some observed images on the above-mentioned rare histologic variants in Chapter 5.

In AK, microscopic changes are confined within the epidermis and initiate in the basal layer. Along the progress of the disease, aggregates of atypical, pleomorphic (多形的) keratinocytes at the basal cells layer would extend to the granular and cornified layers. The epidermis thus demonstrates an abnormal architecture. The dermo epidermal junction appears irregular because of small round buds at the basal cells layer that protrude slightly into the upper papillary dermis. The basal layer of AK often looks closer crowding of atypical keratinocytes than normal basal layer. Hyperkeratosis (角質層增厚) and parakeratosis (角質層角化不完全) are present in AK, the latter overlying the abnormal cells in the epidermis. The thickness of the stratum spinosum of AK is thicker than thickness of normal the stratum spinosum, which is called irregular acanthosis. Moreover, actinic keratoses almost always occur in association with solar elastosis and superficial inflammatory infiltrate in the dermis.

On cytologic grounds alone, AK contains atypical keratinocytes with loss of polarity, with nuclear pleomorphism, with disordered maturation, and with increased numbers of mitotic figures. Many of the keratinocytes are pleomorphic also in the cellular level.<sup>[34]</sup> Fig. 2.3.2.2(a) shows that an actinic keratosis demonstrates atypical keratinocytes along the basal layer with hyperchromatic nuclei and atypical maturation compared with the Fig. 2.3.2.2(b) which is the histology of normal skin. Thus, we

focused on the epidermis (especially the basal layer) in our *in vivo* clinical trials. Based on previous finding, here we summarize (Table 2.3.2.1) the histopathologic features in different epidermis layers, as the diagnosis criterion of our HGM studies of AKs.



Stratum corneum	Parakeratosis/Hyperkeratosis
Stratum granulosum/spinosum	Irregular acanthosis Abnormal architecture Pleomorphisms of cells and nuclei
Stratum basale	Crowding of keratinocytes Abnormal architecture Pleomorphisms of abnormal cells and nuclei
Dermis	Solar elastosis

Table 2.3.2.1 Histopathologic features of AK for diagnosis criterion of H&E and HGM images.

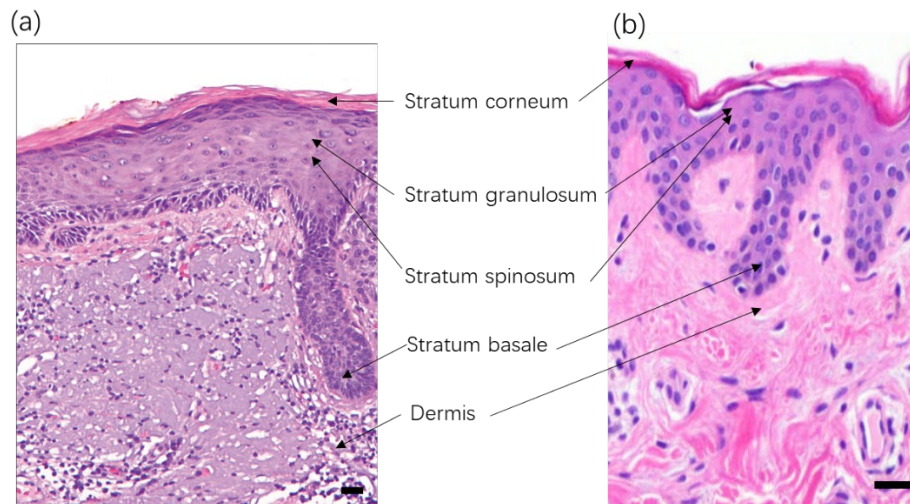


Fig. 2.3.2.2<sup>[35]</sup> (a) Histology (H&E) of AK. (b) Histology (H&E) of normal skin. Scale bar=20 μm. Copyright: J. Lanoue, C. Chen, G. Goldenberg, “Actinic keratosis as a marker of field cancerization in excision specimens of cutaneous malignancies.” *Cutis*. 2016, 2016, 97:6 (415-420) with permission from Wolters Kluwer health, Inc.

### 2.3.3 Comparing AK and Normal Tissues with H&E Examination

Here we show some H&E examination images of AKs, with corresponding features in Table 2.3.2.1. This discussion will assist to form our judgement standard.

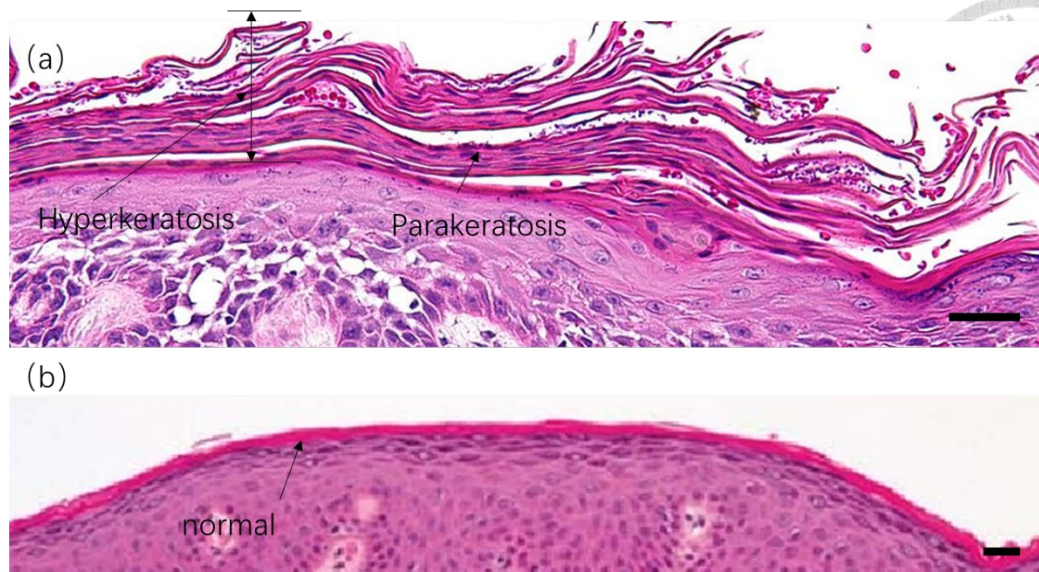
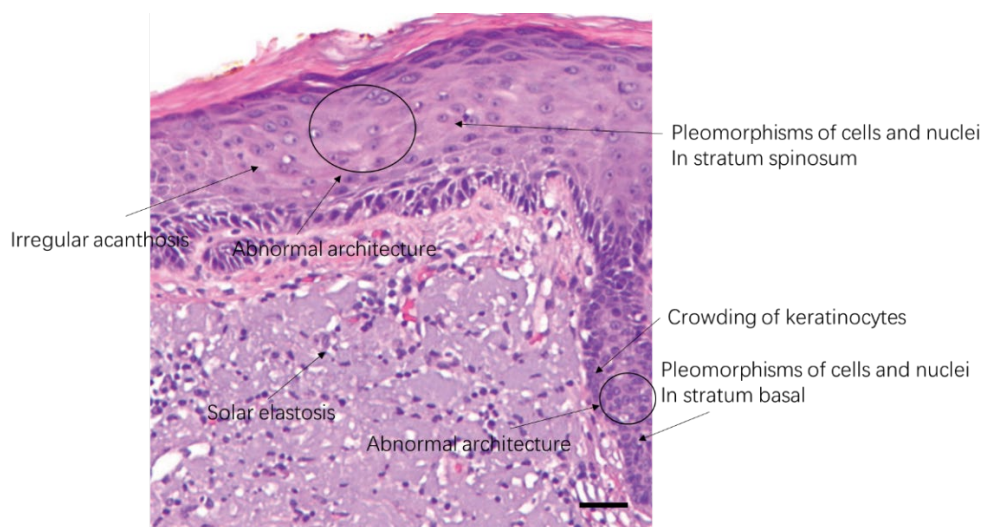


Fig. 2.3.3.1 (a)<sup>[36]</sup> Histology (H&E) of Bowenoid AK in the stratum corneum: parakeratosis/hyperkeratosis in the arrows. Copyright: own work in Wikimedia commons, Nephron. With permission from owner Nephron. (b)<sup>[37]</sup> Histology (H&E) of normal skin in the stratum corneum. Scale bar=20  $\mu$ m. Copyright: A. Day, S. M. Holland, J. P. Scurry, "Normal vulvar histology: variation by site." *Journal of Lower Genital Tract Disease*, 2016, 20:1 (64-69) with permission from Wolters Kluwer health, Inc.

Fig. 2.3.3.1 shows the parakeratosis and hyperkeratosis, in comparison with the normal stratum corneum. From Fig. 2.3.2.2 (b), the thickness of the stratum corneum is one or two cell layers and the nuclei is disappeared. But in Fig. 2.3.3.1(a) keratinization is not complete in the labeled arrow "parakeratosis" due to the retention of nuclei. In the labeled arrow "hyperkeratosis" region, the thickness of the stratum corneum is thicker than the normal one due to proliferation of keratinocytes.



---

Fig. 2.3.3.2 Histology (H&E) of AK. Scale bar=20  $\mu$ m. It is marked the different situations in the stratum spinosum and the stratum basale. Copyright: J. Lanoue, C. Chen, G. Goldenberg, "Actinic keratosis as a marker of field cancerization in excision specimens of cutaneous malignancies." *Cutis*. 2016, 2016 ,97:6 (415-420) with permission from Wolters Kluwer health, Inc.

Fig. 2.3.3.2 shows the irregular acanthosis in the labeled location, where the thickness of the stratum spinosum is thicker than the thickness of the normal stratum spinosum in Fig. 2.3.2.2(b) and these cells are irregular. In Fig. 2.3.3.2, the circles show abnormal architecture in the stratum basale. These cells are in disordered array. Fig. 2.3.3.2 also shows the pleomorphism of cells and nuclei in the stratum spinosum and in the stratum basale. The shape of cells is not oval and cells vary in different size. In the stratum basale, Fig. 2.3.3.2 shows crowding of keratinocytes, where the cells are closer to each other than cells in Fig. 2.3.2.2(b). In the dermis, Fig. 2.3.3.2 shows the solar elastosis, where the elastosis fiber is purple. The normal collagen fiber is pink in the H&E section in Fig. 2.3.2.2(b). If the connective tissue is purple in H&E section, it means that solar elastosis happens. For all these histopathologic features of AK for diagnosis, the features in the stratum basale are the most important because the pathological changes started in the stratum basale in mild AK cases. The stratum corneum and the stratum spinosum are normal sometimes. For diagnosis in reality, the morphology of the stratum basale is also the main standard for pathologist.

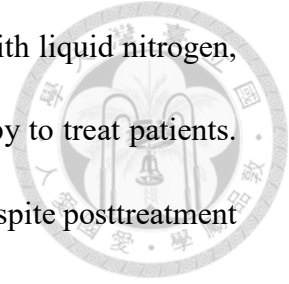
## 2.3.4 Treatment

A variety of treatment options exist for AK, and the method most suitable varies depending on the size, location, and growth of the lesions, as well as on personal



---

preference. The most common treatment options are cryotherapy with liquid nitrogen, fluorouracil, and curettage. In our *in vivo* trials, we used cryotherapy to treat patients. This treatment requires no anesthetic, and patients tolerate it well despite posttreatment swelling and blistering. The recurrence rate of AKs with this method, while unknown, appears to be low and has been estimated to be as low as 1.2%.<sup>[38]</sup>



---

## Chapter 3      Optical Tracking System Setup



### 3.1 3D Camera Tracking System

Most patients get more than one AK and new AKs will continue to appear for life. Early on, they may disappear only to reappear later. For comparing the effect of treatment, the same positions of AK lesions are also necessary. So, we should track the same lesion position for longtime. Moreover, we also want to record the all multiple locations of AK lesions. Common cameras only record 2D information and the location information cannot be the same in 3D coordinates, which means that we might not be able to take the HGM images in the same location after treatment. In same time, it is also not convenient for record the location of lesion one by one. Furthermore, with 3D coordinate information it is possible to achieve automatic diagnosis by mechanical arm and AI. It is a fundamental and meaningful work for future. In our lab, we first use 3D camera to scan the head of patients to record the AK lesions. Our 3D camera is EinScan-Pro made by SHINING 3D shown in Fig. 3.1.1. The 3D camera can capture textured and colored objects ranging in size from 0.03 m (.0011 in) up to 4 m (13 ft). The scan speed is 10 frames/s. Moreover, whole scanning time is less than 2 mins due to the old patients. The image processing software is Mesh lab.



Fig. 3.1.1 3D Camera: EinScan-Pro.

When we use the 3D camera every time, we should perform the camera calibration.

The step is shown in Fig. 3.1.2.

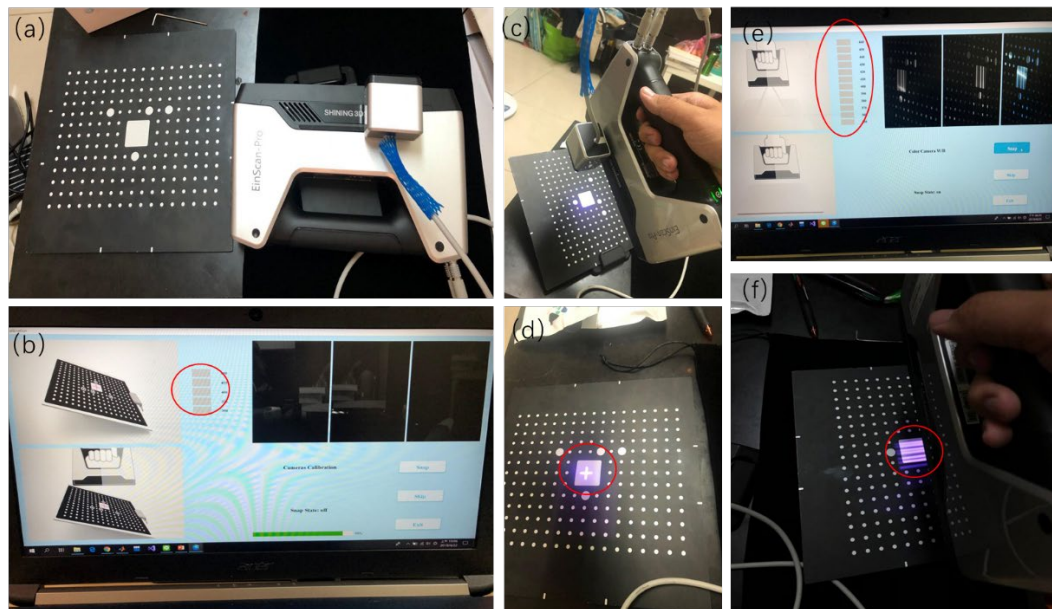


Fig. 3.1.2 (a) 3D Camera-EinScan-Pro 3D camera and the calibration plate. (b) The operation window with calibration step 1. Gray plaids need to be lighted on in the red circle. (c) The calibration plate is set obliquely. The camera shoots a purple cross of light to the white area. (d) The purple cross of light in the white area. (within the red circle) (e) The operation window with calibration step 2. Gray plaids need to be lighted on shown as in the red circle. (f) The camera shoots purple lines (in the red circle) of light to the white area.

The first step is to set the calibration plate obliquely and then the camera shoots a purple cross of light. We should focus the cross of light on the white area (the red circle shown in Fig. 3.1.2.(d)) and move the camera far and near to the plate, which lights all the gray plaids on (the red circle shown in Fig. 3.1.2.(b)). Moreover, we should repeat

---

the same process in four directions of the calibration plate and then the calibration step 1 is finished. In calibration step 2, we place the calibration plate horizontally on the desk first and then the camera shoots purple lines of light (the red circle shown in Fig. 3.1.2.(f)). Similar to step 1, we should focus the lines on the white area and move the camera far and near to the plate, which lights all the gray plaids on (Gray plaids are shown in the red circle in Fig. 3.1.2.(e)). After 2 steps, the calibration is finished.

Before we take 3D images of volunteers, we should let them wear eye masks. In next, we should make them sit down and keep still. When we start to take 3D image, we should scan the whole face of the volunteer stably until the image is complete in the computer. The whole process of scanning is usually limiting in 2 mins.

## 3.2 Optical System Setup

The system setup of the harmonic generation microscopy (HGM) for the AK clinical trial is shown in Fig. 3.2.1 to Fig. 3.2.3. In the whole system, we utilized a Cr:forsterite laser with a wavelength of 1260 nm, a bandwidth of 90 nm, a pulse width of 48 fs, average power in mode-locked of 605mW and a repetition rate of 105 MHz as the excitation source. The laser beam was collimated by a pair of cylindrical lenses to optimize the beam shape and by a chirped mirror pair to compensate the group velocity dispersion. The beam after passing through a ND wheel to attenuate the power to a safe level for clinical studies was guided into a galvo-resonant scanning head (Thorlabs Laser Scanning Essentials Kit) to perform 2D-scanning. Next, the laser beam was

---

focused by an infrared water immersion objective (UAPON340/40X/NA=1.15, Olympus, Tokyo, Japan) with a working distance of 250  $\mu\text{m}$  to excite nonlinear signals in skin. By focusing the laser excitation beam underneath the skin surface, SHG signals at a wavelength of 630 nm and THG signals at a wavelength of 420 nm were generated at the laser focus and the signals originated from the excitation focus were epi-collected and collimated by the same objective and a dichroic beam splitter (DBS). THG and SHG signals were divided by another DBS and sent to two photo-multiplier tubes (PMT) for signal detection (Hamamatsu R4220P for THG and Hamamatsu R928P for SHG). Before PMTs, they were filtered by two band-pass filters (D410/30 for THG and D615/10 for SHG) inserted. The objective was attached to a 3D step motor so that the position of the objective could be adjusted by both manual tuning and electrical control.

It is reported that conversion efficiency of SHG is  $\sim 2.0 * 10^{-7}$  and conversion efficiency of THG is  $\sim 1.4 * 10^{-9}$  in biological skin tissue.<sup>[39]</sup> In our system, the radiant sensitivity of PMT is  $7.4 * 10^5$  A/W. The background noise is mainly caused from dark current (3 nA). The pixel intensity of background noise is 100 while the pixel intensity of THG is 4000 and the pixel intensity of SHG is 10000. So, the conversion efficiency of SHG is at least  $\sim 4.1 * 10^{-12}$  and the conversion efficiency of THG is at least  $\sim 1.6 * 10^{-12}$ .

An objective adapter (shown in Fig. 3.2.3(c)) with a cover glass was attached between objective and human skin. Water was dropped in the adapter due to the requirement for the water-immersed objective. Inside the adapter the objective could be moved vertically to take images at different depths.

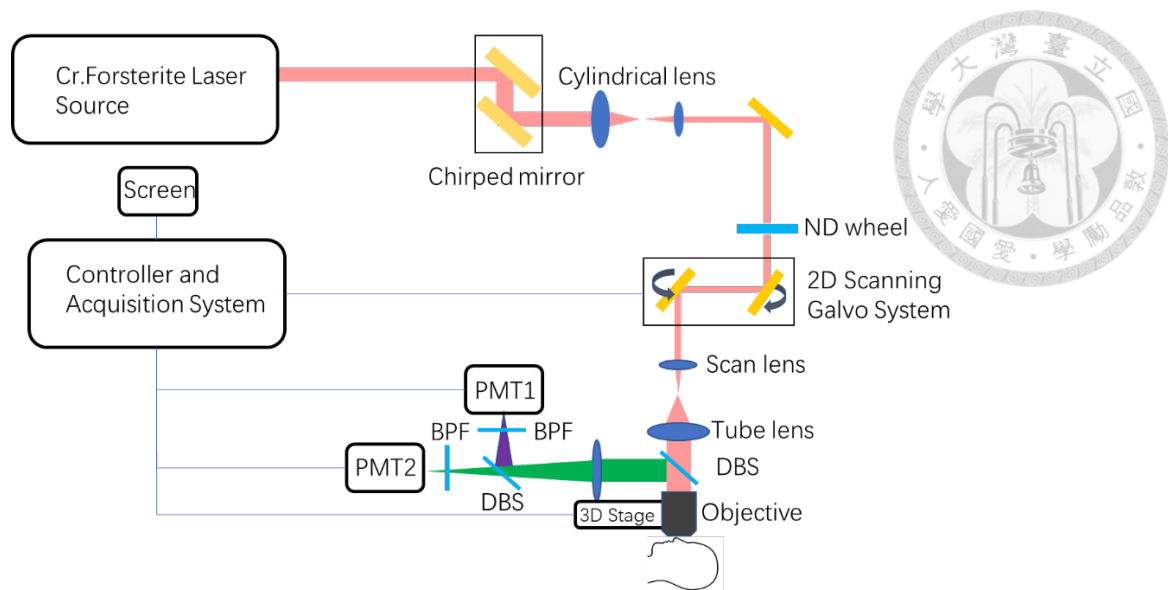


Fig. 3.2.1 A schematic diagram of the optical harmonic generation microscopy system used in the clinical trials. DBS: dichroic beam splitter; PMT: photomultiplier tube; BPS: band-pass filter.

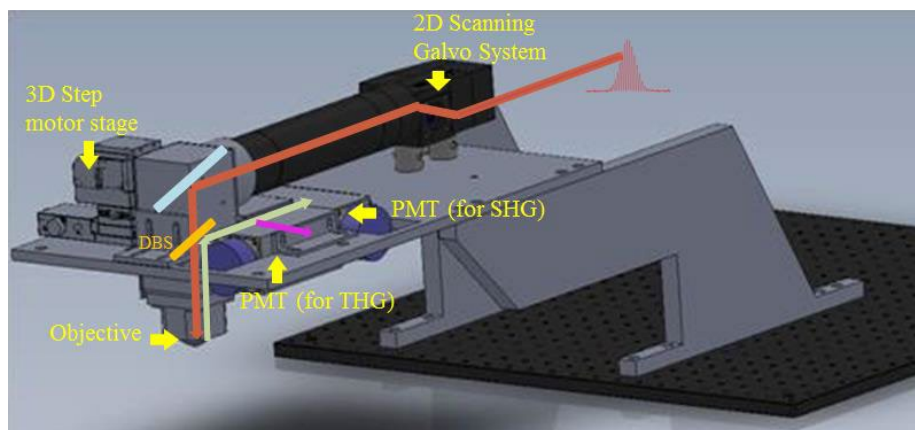


Fig. 3.2.2 The mechanical structure of the optical harmonic generation microscopy system. DBS: dichroic beam splitter; PMT: photomultiplier tube; SHG: second harmonic generation; THG: third harmonic generation.

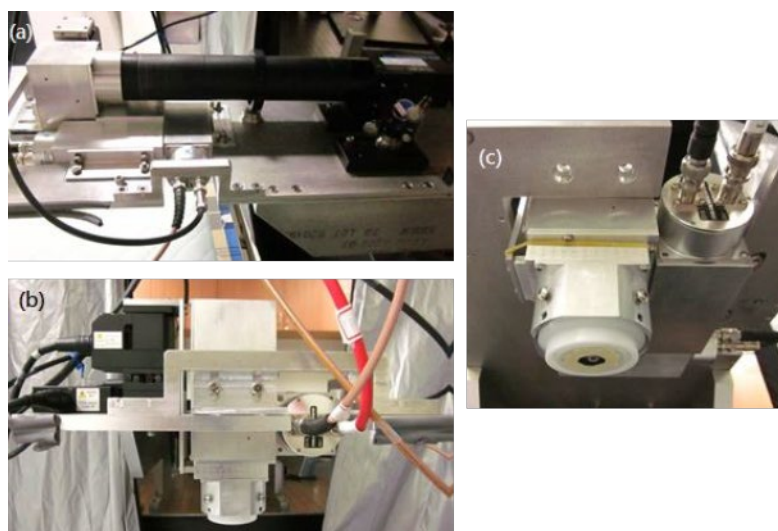


Fig. 3.2.3 Photos of the harmonic generation microscopy system. (a) Side view. (b) Front view. (c) Upward front view.



### 3.3 Movable Optical System Setup

Due to the shaking of patients, we further developed the optical harmonic generation microscopy system to be movable shown as Fig. 3.3.1.

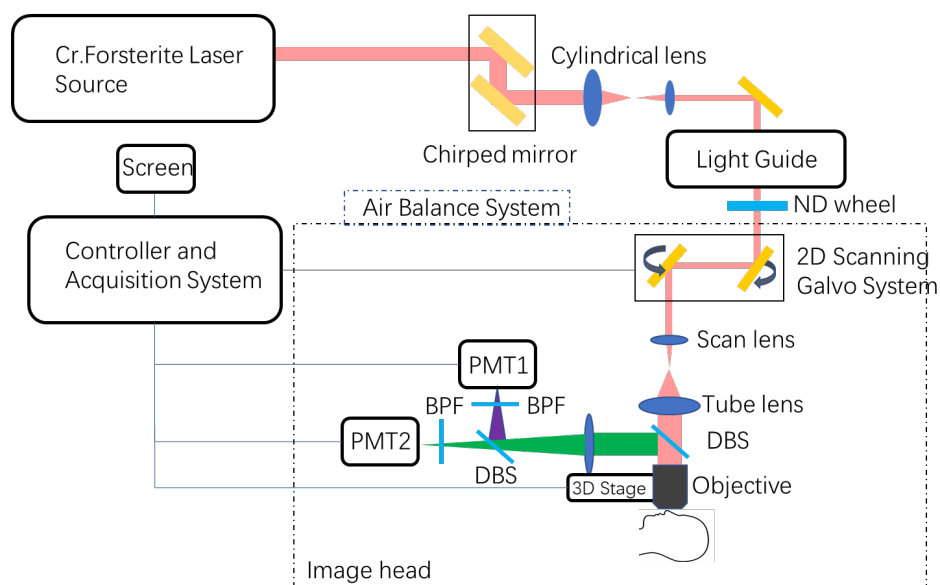


Fig. 3.3.1 A schematic diagram of the movable optical harmonic generation microscopy system with a light guide. DBS: dichroic beam splitter; PMT: photomultiplier tube; BPS: band-pass filter.

We redesigned the mechanical structure of optical harmonic generation microscopy system to integrate scanning systems into a box called “image head”. Air-pressure-based antigravity arm was responsible for holding the whole image head, which could move in 3 directions flexibly. The maximum movement range in x-y-z is 30 cm \* 30 cm \* 30 cm. To align the laser beam always into the image head in the same direction and position with the movement of whole system, a light guide containing 8 reflective mirrors was integrated. Therefore, the whole system could be moved with the shaking of patients while the relative position of the objective and the lesion is stabilized, which makes the image still legible. The mechanical structure of image head is shown as Fig. 3.3.2 and the whole system in reality is shown as Fig. 3.3.3.

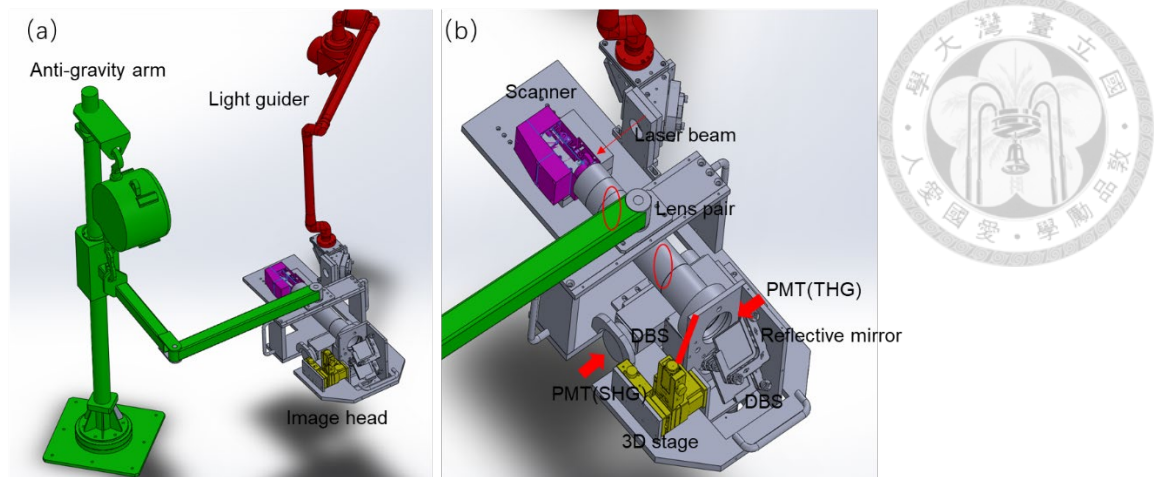


Fig. 3.3.2 (a) The mechanical structure of the optical harmonic generation microscopy system. Light guide and anti-gravity arm are integrated with an image head. (b) The detailed mechanical structure of the image head. DBS: dichroic beam splitter; PMT: photomultiplier tube; SHG: second harmonic generation; THG: third harmonic generation.

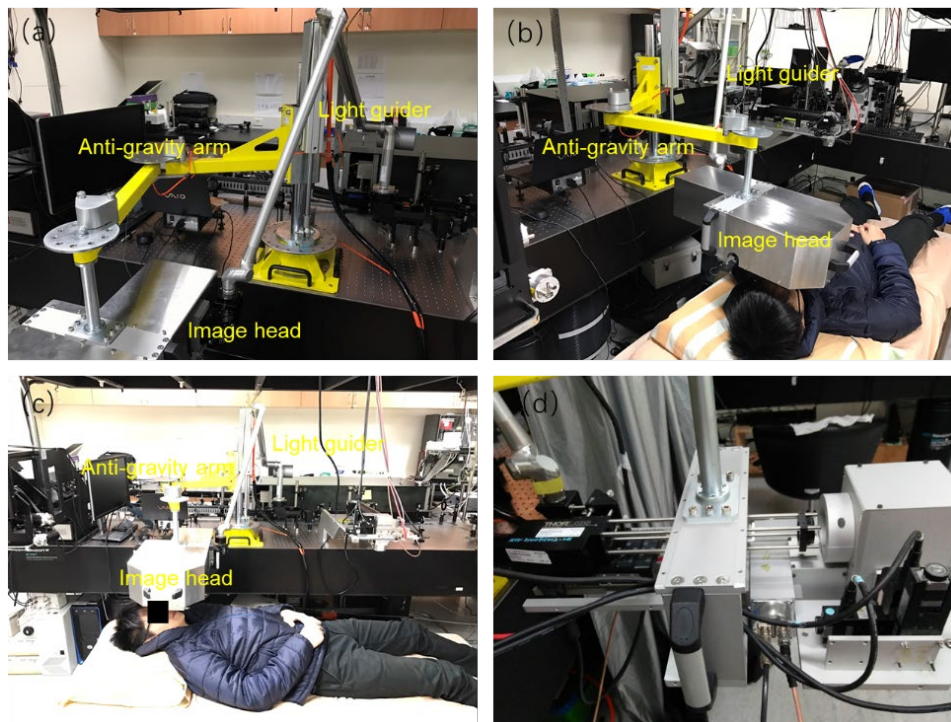
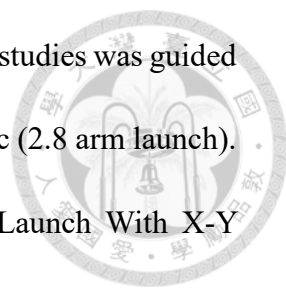


Fig. 3.3.3 The whole system in reality. (a) Down view. (b) Side view. (c) Front view. (d) Image head.

In the new system, we still utilized the Cr:forsterite laser with a wavelength of 1260 nm, a bandwidth of 90 nm, a pulse width of 48 fs, average power in mode-locked of 605mW and a repetition rate of 105 MHz as the excitation source. The laser beam was collimated by a pair of cylindrical lenses to optimize the beam shape and by a chirped mirror pair to compensate the group velocity dispersion. The beam after passing



---



through a ND wheel to attenuate the power to a safe level for clinical studies was guided into the light guide. The light guide was from Laser Mechanisms, Inc (2.8 arm launch). The process of light guide alignment is in handbook “2.8 Arm Launch With X-Y Adjuster” and we will introduce the alignment procedure at the end of this sub-section. The movement range of the light guide was 30 cm X 30 cm X 30 cm in x-y-z directions respectively. The passing rate @1260 nm of light guide with 8 reflective mirrors was more than 96% and the angler bias of the light guide was 0.7 mrad. Then laser beam went into a galvo-resonant scanning head (Thorlabs Laser Scanning Essentials Kit, MPM2PKIT) to perform 2D-scanning. It was 8 kHz resonant scanner. In Fig. 3.3.2 (b), the reflective mirror was silver mirror (ME1S-P01, Thorlabs). The DBS below the reflective mirror was a long-pass dichroic beam-splitter (DMLP900R, Thorlabs). The DBS near the PMTs was a long-pass dichroic beam-splitter (DMLP550R, Thorlabs) while the mount of this DBS was a rotating platform (B3CR, Thorlabs). The objective (UAPON340/40X/NA=1.15, Olympus, Tokyo, Japan) was still with a working distance of 250  $\mu\text{m}$  and PMTs were Hamamatsu R4220P for THG and Hamamatsu R928P for SHG. Before PMTs, two band-pass filters were D410/30 (CHROMA) for THG and D615/10 (CHROMA) for SHG. The field of view (FOV) of the new moveable system was 235  $\mu\text{m}$  \* 235  $\mu\text{m}$ . The lateral resolution was 395  $\mu\text{m}$ , whose theoretical resolution was 328  $\mu\text{m}$ .

To align the light guide with laser beam, we should do the followings.

1. We should make the laser beam parallel to optical table.
2. We should move the launch of light guide accurately to match the laser beam into

---

the center of launch and set an iris in front of the launch.

3. We should record a position of laser beam in the far distance (ex. iris or cross target in the wall).
4. After blocking the original laser beam, we should put the He-Ne laser source in the launch and make the He-Ne laser beam through the recording position in step 2 and step 3. It means that the He-Ne laser beam matches the original laser beam.
5. We should align light guide with He-Ne laser beam. The detector tool is duma (He-Ne laser beam detector) containing a target lens. Duma connects to the computer and the software is SpotOn. We remove the first reflective mirror of light guide arm and set the detector instead shown in Fig. 3.4.4 (a). Fig. 3.4.4 (a) is the sketch of alignment with duma. The purpose is to align the He-Ne laser beam through duma with designing angle and position of light guide by adjustment screws.
6. The adjustment screws are shown in red circles in Fig. 3.3.4 (b). Screws shown in the circles 1 are used to adjust the angle of the mirror and screws shown in the circles 2 are used to adjust the relative position between duma and He-Ne laser beam shown in the double-headed arrow in Fig. 3.3.4 (b). We should see a cross drawing a semicircle in screen (shown in Fig. 3.3.4 (c)) when rotating the light guide arm  $180^\circ$  in scale  $200\ \mu\text{m}$ . By adjusting screws (circles 1 in Fig. 3.3.4 (b)), we should move the cross to the center of the semicircle.
7. Then we should remove the target lens in the duma and repeat step 5 with adjustment screws (circles 2 in Fig. 3.3.4 (b)).
8. Next, we should repeat the step 6 and 7 in different zooms ( $200\ \mu\text{m}$ ,  $100\ \mu\text{m}$ ,  $50$



$\mu\text{m}$ ). The smallest scale we should use is  $50 \mu\text{m}$ .

9. The alignment is finished when the cross cannot draw a semicircle.

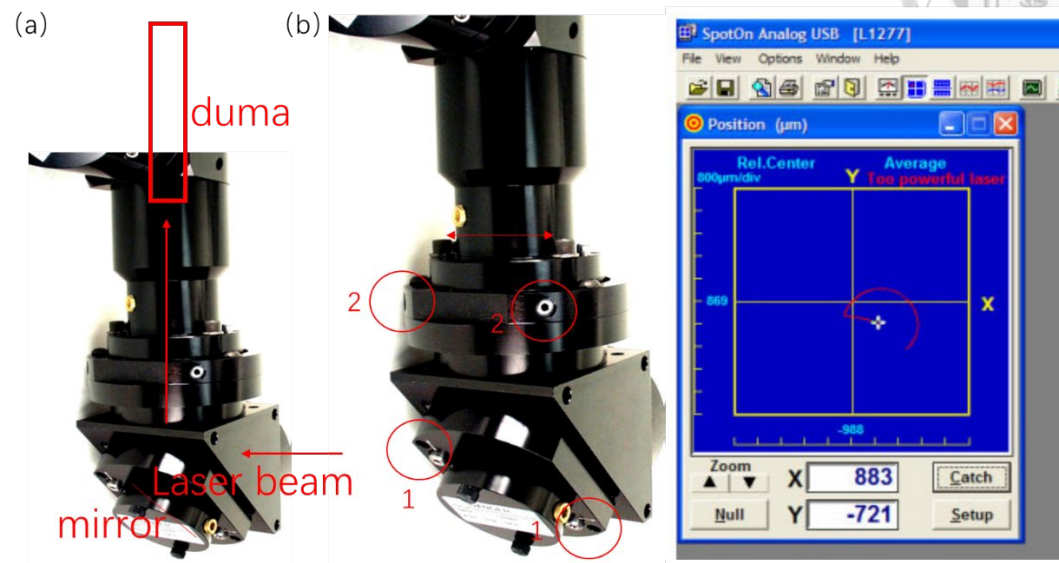


Fig. 3.3.4 (a) The sketch of alignment with duma. (b) Two adjustment screw pairs in the circles 1 and 2 in a part of light guide. (c) A small cross drawing a semicircle on the screen.

# Chapter 4 Materials and Methods



## 4.1 Protocol of the Clinical Trial

This clinical trial was approved by the National Taiwan University Hospital Research Ethics Committee (No. 201606136DINB). The whole study involved 5 Asian volunteers with multiple AKs (1 *ex vivo* and 4 *in vivo*), where the details are shown in Table 4.1.1. The diagnosis of AK was made by a dermatologist Prof. Yi-Hua Liao. We also collected one volunteer as the normal comparison. This volunteer is from the IRB case No. 201612113DINC.

Case	Sampling	Age	Sex	Location
AK patient 00	<i>Ex vivo</i>	81	Male	Skull, cheek
AK patient 01	<i>In vivo</i>	93	Male	Skull
AK patient 02	<i>In vivo</i>	70	Female	Cheek
AK patient 03	<i>In vivo</i>	85	Female	Cheek
AK patient 04	<i>In vivo</i>	91	Male	Cheek
The normal volunteers	<i>In vivo</i>	70	Female	Cheek

Table 4.1.1 Information of volunteers.

The protocol of the clinical trial in shown in Fig. 4.1.2.

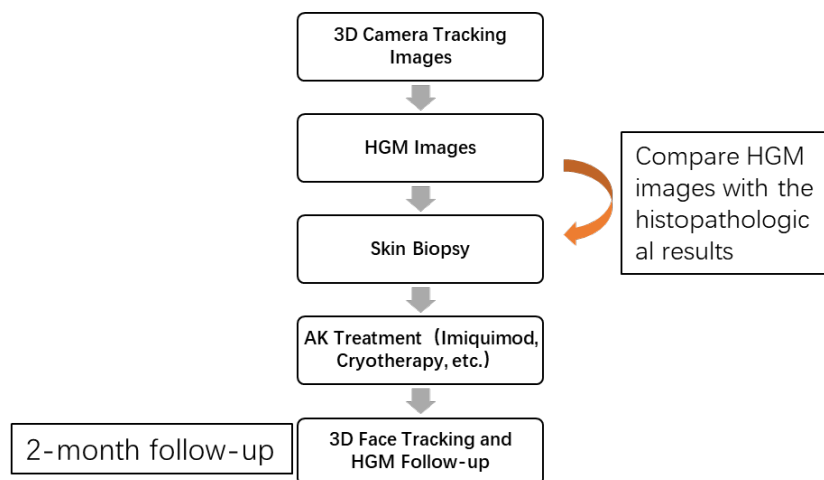
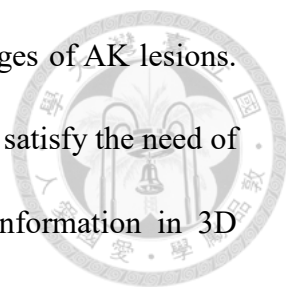


Fig. 4.1.2 The protocol of the whole clinical trial.

---



First, we used the 3D camera tracking system to take 3D images of AK lesions. Because the lesion was not in the same height, 2D images could not satisfy the need of surface area measurement. And also, 3D images could record information in 3D coordinates, thus avoiding the variation in photo-taking angles. Then, we took up to three image stacks for the AK lesion (The lesion is pointed by the doctor.) with HGM. For each image stack, the process of imaging is less than 1 minute. With less than nine AK sites plus one normal site, the total exposure time of the laser light for each volunteer was less than 10 mins. With an average excitation power after the objective around but slightly less than 100 mW, the accumulated photon energy would be less than 60 J in each volunteer, well within the laser safety region.<sup>[40][41]</sup> The lesion we have taken HGM images was later-on skin biopsied (not the whole lesion) and then we compared the two types of images to find the comparison results. This step was aimed at studying if the HGM images can assist diagnosis of AK without biopsy. Next, patients got treatment (cryotherapy) in the lesion we took and we repeated taking 3D images and HGM images in two months after the treatment.

## 4.2 Image Acquisition

There were two types images we have taken: 3D facial images and HGM images. For recording the all AK lesions, we used the 3D camera to scan the whole face of volunteer. The volunteer would be asked to sit down and wear eye shields. The process was less than 2 mins.

---

In next, we would take HGM images of AK lesions pointed by doctor. In order to ensure that the HGM images were acquired from AK lesions, a thin plastic ring with a hollow circle approximately of the size of the lesion was stuck on the subjects' face (shown in Fig. 4.2.1 (a)). The SHG and THG signals would not be generated under the opaque plastic ring. When taking the HGM images, the volunteer would be asked to lie on an electric hospital bed with its height and bending angle adjustable (shown in Fig. 4.2.1 (b)). The environment of lab would be absolutely dark due to the working condition of PMTs. Because the AK volunteers were aged, the whole process of taking HGM images would be less than 30 mins. To control the condition of each experiment, there were some parameters to be determined. First, the excitation power after the objective should be measured before attaching the white adapter to make sure that it was around 100 mW. Second, the PMTs voltage, determining the amplification level of the signal, should be set at a certain level. For SHG modality, the voltage was set as 600 volts. For THG modality, the voltage was set as 700 volts. Finally, the step size along the optical axis of the automated step motor to which the objective was attached was set as 1.8  $\mu\text{m}$ . During the acquisition, the software ThorImageSL 3.0 would be set to 512 \* 512 pixels.

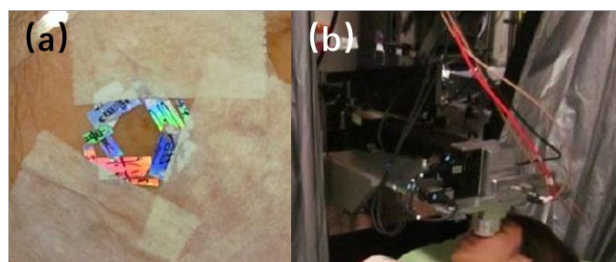


Fig. 4.2.1 (a) The illustration on how a plastic ring was used to prevent acquiring images outside the lesion. (b) The electric hospital bed with a volunteer.

# Chapter 5 Results and Discussion



## 5.1 Images of the 3D Tracking System

With 3D camera system, we recorded images of 4 patients (AK patients 01 to 04) as shown in

Fig. 5.1.1, Fig. 5.1.2 and Fig. 5.1.3.



Fig. 5.1.1 3D camera images of AK 01 patient's lesion. (a) AK lesion area is 4.835 cm<sup>2</sup>. (Location in yellow marked.) (b) The length of AK lesion is 2.351 cm. (c) The width of AK lesion is 0.861 cm.

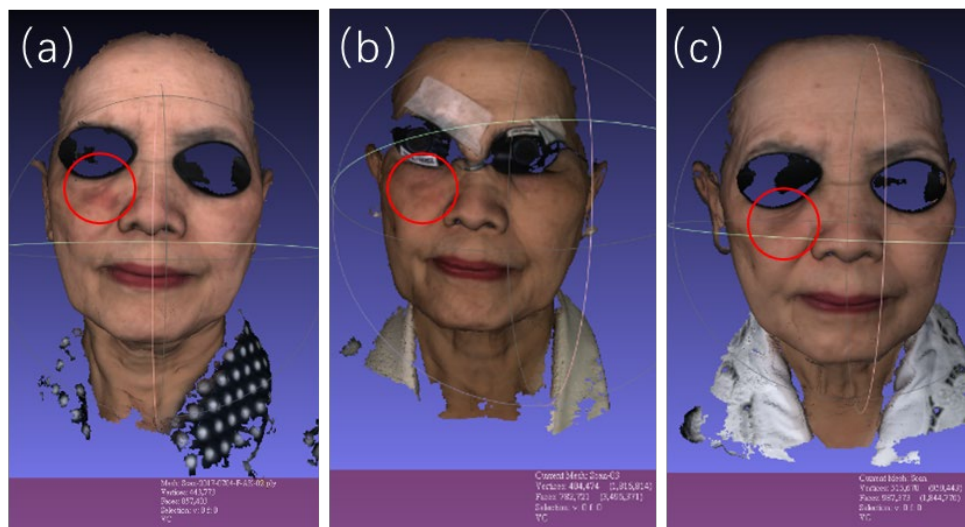


Fig. 5.1.2 3D camera images of AK 02 patient's lesion. (a) The location and clinical presentation of the AK lesion before treatment (red circle). (b) The location and clinical presentation of the AK lesion 2 months after treatment (red circle). (c) The location and clinical presentation of the AK lesion 4 months after treatment (red circle).

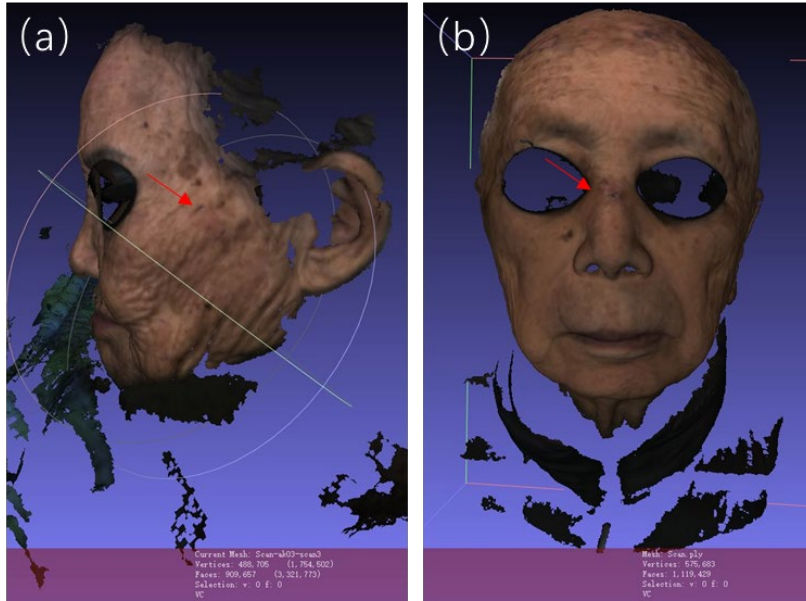


Fig. 5.1.3 (a) 3D camera images of AK 03 patient's lesion. The location of AK is marked with a red arrow. (b) 3D camera images of AK 04 patient's lesion. The location of AK is marked with a red arrow.

In Fig. 5.1.1(a), we can calculate that the specific lesion area on a curved surface was  $4.835 \text{ cm}^2$  accurately. The feature and location of lesion is distinct compared to the normal photos. Fig. 5.1.2 shows that the lesion of AK patient 02 got flatten and pale after treatment. Fig. 5.1.3 shows location of lesion on the cheek of AK patients 03 and 04.

## 5.2 Images of HGM

The whole clinical trial contains 5 patients (AK patient 00 to 04), including 1 *ex vivo* and 4 *in vivo*. We show the *en face* sectioned HGM images of normal volunteer first. In next, we show the results of 5 patients case by case.



---

## 5.2.1 Normal Epidermal Images of HGM



Normal epidermal stratification of the stratum corneum, the stratum granulosum, the stratum spinosum, and the stratum basale can be visualized in serial *en face* label-free virtual sections by using HGM and has already been described before.<sup>[42]</sup> Thus, a stack of HGM images of normal epidermal on face shown in Fig. 5.2.1.1 are used as our standard for comparison. In other words, these images are used to compare with the results of 5 patients in the morphology as will be discussed below. In Fig. 5.2.1.1, we can see different layers in different depths where the morphology is consistent with Fig. 2.3.2.2(b). The thickness of the normal stratum corneum in face is  $9(\pm 2) \mu\text{m}$ .<sup>[43][44]</sup> If the thickness of the stratum corneum we measured is more than  $11 \mu\text{m}$ , it would suggest hyperkeratosis. In stack of Fig. 5.2.1, the distance between each picture in z direction is  $0.6 \mu\text{m}$  while the whole stratum corneum contains 15 pictures. So, the thickness of the stratum corneum in our normal comparison is  $9 \mu\text{m}$ , less than theoretical value. The thickness of the stratum spinosum depends on where it is located on the body.<sup>[45]</sup> So, we use the thickness we measured in our normal volunteer. The thickness of our normal stratum spinosum is  $16.2 \mu\text{m}$  (27 pictures). If the thickness of the stratum spinosum we measured is more than  $19 \mu\text{m}$  (20% more), it would suggest irregular acanthosis.

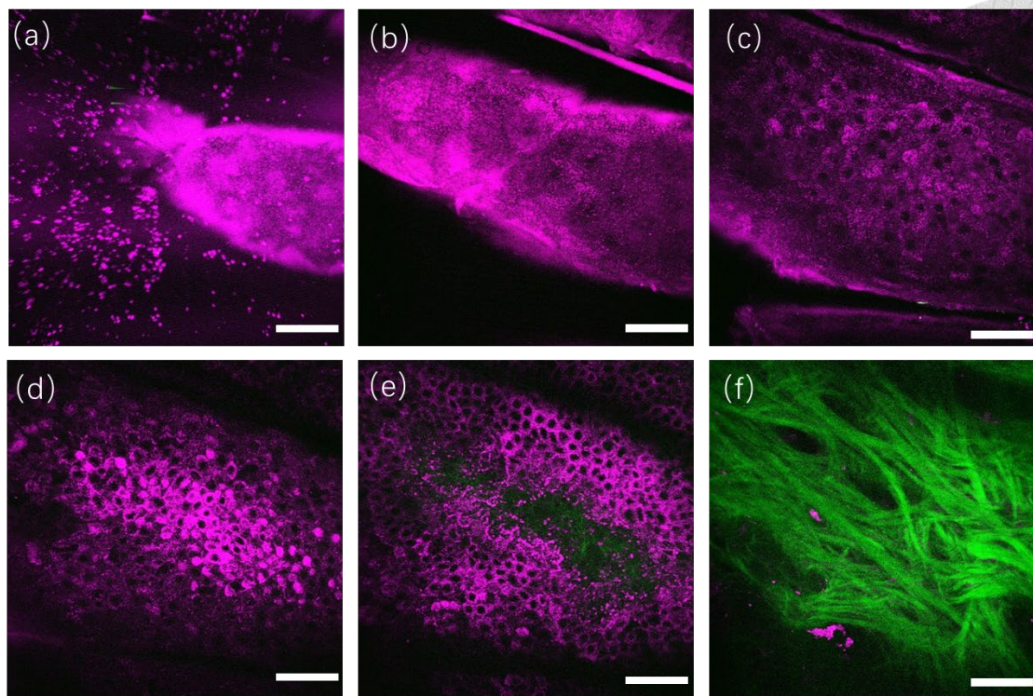


Fig. 5.2.1 [(a) to (f)] A representative series of *in vivo* HGM images at different depths relative to the surface (5.4, 14.4, 30.6, 52.2, 75.6 and 111.6  $\mu\text{m}$ ). (a) Stratum corneum. (b) Stratum granulosum. (c) Stratum spinosum. (d) and (e) Stratum basale. (f) Dermis. Scale bar=50  $\mu\text{m}$ .

## 5.2.2 Result of the AK Patient 00

Following the evaluation standard in Table 2.3.2.1, Fig. 5.2.2.1 exemplifies the H&E histopathology of the AK patient 00 in a transverse section, whereas Fig. 5.2.2.2 illustrates representative *en face* optically-sectioned HGM images of the same AK lesion, at depths in the epidermis that correspond to the lettered lines (a, b, c, d, e, f) in Fig. 5.2.2.1. For easier and clearer to explain, we show histopathology details in labeled Fig. 5.2.2.3.

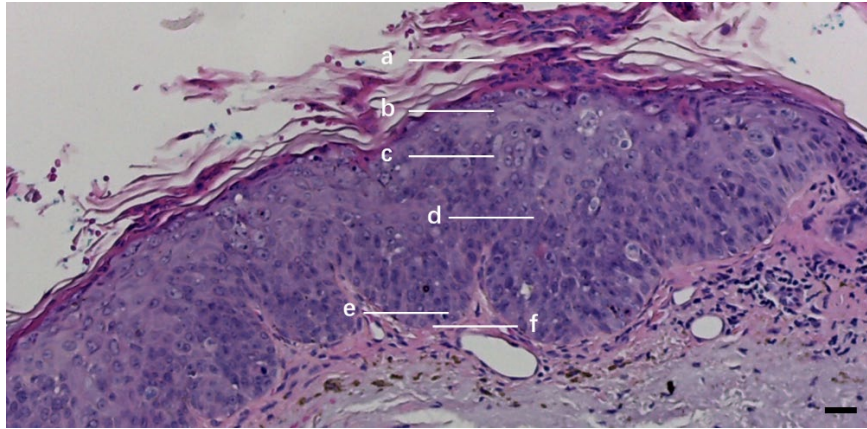


Fig. 5.2.2.1 A transverse histopathology section of the AK patient 00 on the skull. Lines a, b, c, d, e and f represent depths in the epidermis corresponding to *en face* sections in Fig. 5.2.2.2. Line a is in the stratum corneum. Line b is in the stratum granulosum. Lines c and d are in the stratum spinosum. Line e is in the stratum basale and line f is in the dermis. Scale bar=10  $\mu$ m.

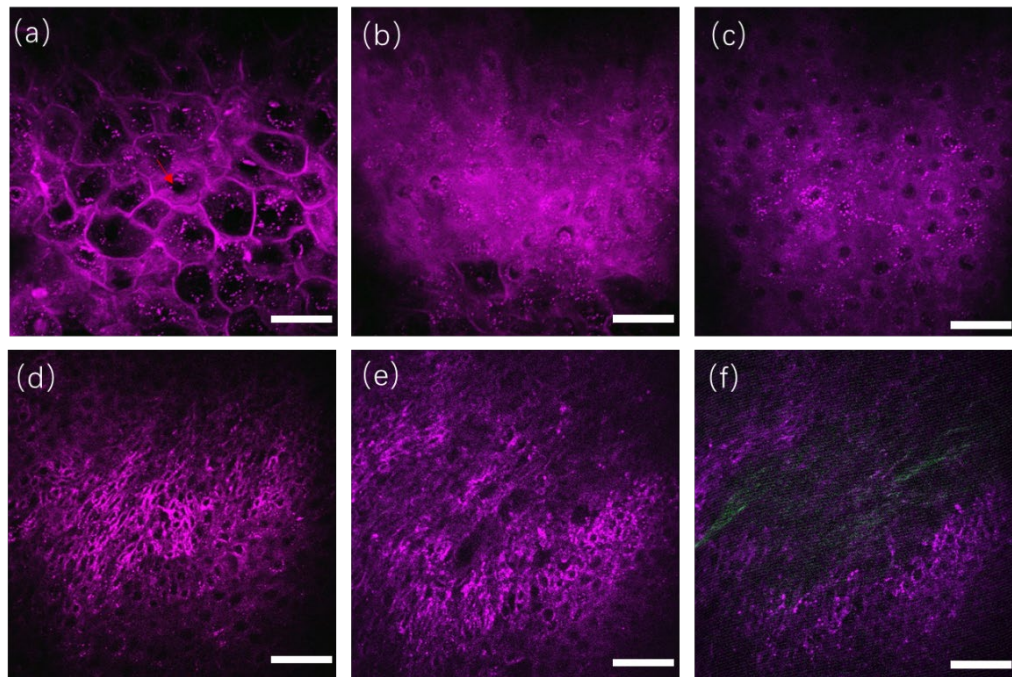
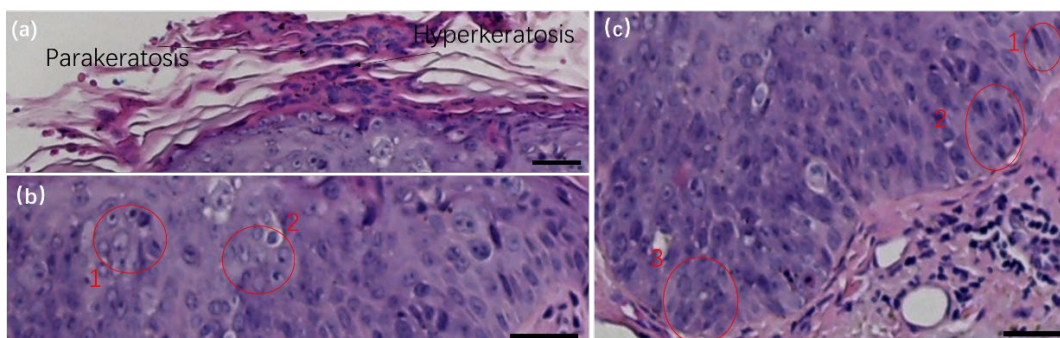


Fig. 5.2.2.2 Actinic keratosis [(a) to (f)] A representative series of *ex vivo* HGM *en face* sectioned images at different depths relative to the surface (24, 90, 127, 199, 233 and 248  $\mu$ m) in AK patient 00. The lesion is on the skull. (a) Stratum corneum. There are nuclei (black hole) in the red arrow. (b) Stratum granulosum. (c) and (d) Stratum spinosum. (e) Stratum basale. (f) Dermis. Scale bar=50  $\mu$ m.



---

Fig. 5.2.2.3 A transverse histopathology section of the AK patient 00 on the skull. (a) Stratum corneum. Parakeratosis and hyperkeratosis are obvious to see. The thickness of the stratum corneum is thicker than normal one. (b) Stratum granulosum and stratum spinosum. These cells are all in different sizes and abnormal architecture. Irregular acanthosis is noted in the stratum spinosum. In the circle 1, the pleomorphism of nuclei is in the cell and cells are in different sizes. In the circle 2, the cell losses polarity and they are irregular acanthosis. (c) Stratum basale. Abnormal architecture is in the stratum basale. The cells are in different sizes and shapes crowding to each other. In the circle 1, the basal cells are slender and bending not like the normal ellipse. In the circle 2, cells are in pleomorphism. In the circle 3, cells are crowding to each other and in different sizes. Scale bar=10  $\mu\text{m}$ .

From the H&E histopathologic features of AK patient 00, some conclusions can be made from Fig. 5.2.1, Fig. 5.2.2.1, Fig. 5.2.2.2 and Fig. 5.2.2.3.

(1) The thickness of the stratum corneum in H&E images of AK patient 00(Fig. 5.2.2.1(a)) is much thicker than the thickness of the normal stratum corneum shown in normal H&E images (Fig. 2.3.2.2(b)). It's hyperkeratosis. The nuclei are still in the stratum corneum. Parakeratosis is obvious. In HGM images of AK patient 00 (Fig. 5.2.2.2(a)), the stratum corneum is 33.6  $\mu\text{m}$  thick (56 pictures), which is much thicker than 11  $\mu\text{m}$ .HGM thus suggests hyperkeratosis. Moreover, the nuclei shown as a dark hole in Fig. 5.2.2.2(a) are still in keratinocyte of the stratum corneum, different from Fig. 5.2.1(a). HGM thus also suggests parakeratosis.

(2) In H&E images of AK patient 00 (Fig. 5.2.2.3(b)), the stratum spinosum shows architectural disarray and cytologic atypia with large and pleomorphic nuclei and cells. In the circle 1, pleomorphism of nuclei happens and cells are in different sizes and shapes. In the circle 2, the cell losses polarity and the thickness of the stratum spinosum is thicker than normal one. It is irregular acanthosis. In *ex vivo* HGM images (Fig. 5.2.2.2(c) and (d)), the thickness of the stratum spinosum is 55.8  $\mu\text{m}$  (93 pictures), which is much thicker than 19  $\mu\text{m}$ . HGM thus suggests irregular acanthosis. Furthermore, in HGM images (Fig. 5.2.2.2(d)), it shows architectural disarray and

---

cytologic atypia with large and pleomorphic nuclei and cells different from normal one in Fig. 5.2.1(d). It reveals abnormal architecture and pleomorphism of cells and nuclei.

In HGM images, the morphology of stratum spinosum can be clearly recognized and is in consistency with H&E histopathology images (Fig. 5.2.2.3(b)).

(3) In the H&E histopathology image (Fig. 5.2.2.3(c)), the stratum basale still shows architectural disarray and cytologic atypia with large and pleomorphic nuclei and cells. The cells are close crowding to each other. In the circle 1, the basal cells are slender and bending rather than oval. Similar morphology can also be observed in HGM images (Fig. 5.2.2.2(e) and Fig. 5.2.2.2(f)). In the circle 2, cells are in pleomorphism. In the circle 3, cells are crowding to each other and in different sizes. Similar morphology (architectural disarray) can also be observed in HGM images (Fig. 5.2.2.2(e) and Fig. 5.2.2.2(f)), different from normal (Fig. 5.2.1(f)), where basal cells are oval rather than slender and bending as shown in Fig. 5.2.2.2(f). Moreover, basal cells in Fig. 5.2.2.2(f) are more crowding to each other than cells in Fig. 5.2.1(f).

(4) In the dermis, H&E image shows solar elastosis. Partial connective tissues in the dermis are purple in Fig. 5.2.2.1. When solar elastosis happens, the deposition of elastin material will increase in the dermis so that it should enhance the intensity of THG signal.<sup>[46]</sup> We choose the HGM images (only retaining THG signals and shown as THG images) which only contains connective tissues in the dermis and measure all area of THG signals. Because the back ground noise is different in different PMTs, we chosen the normal HGM images as comparison with the same PMTs and same PMT settings (THG: 600v). The HMG images of the normal volunteer was from different

---

time and it contained significant noise. So, we reduced the pixel intensity of noise shown in Fig. 5.2.2.4. The normal HGM images only contain signals of connective tissues in the dermis. This picture is the 10<sup>th</sup> layer after the cell structures are disappeared absolutely (reduced the noise). For the HGM image of AK patient 00, the picture is also the 10th layer after the stratum basale is disappeared absolutely. We calculated pixel intensity of the whole image. The abscissa axis is the horizontal position of the image while the vertical axis is the average pixel intensity of each vertical line of the image. As a result, *ex vivo* HGM images show much increased THG intensity (Fig. 5.2.2.5). Fig. 5.2.2.5 (a) shows the THG image of normal connective tissue and Fig. 5.2.2.5 (b) shows the intensity of THG signal of normal connective tissues. Fig. 5.2.2.5 (c) shows the THG image of connective tissue of AK patient 00 without SHG signal and Fig. 5.2.2.5 (d) shows the corresponding intensity of the THG signal.

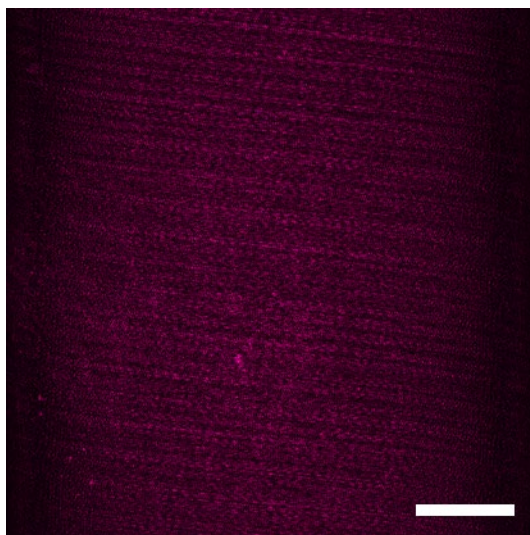


Fig. 5.2.2.4 The noise HGM image of the normal volunteer. Scale bar=50  $\mu$ m.

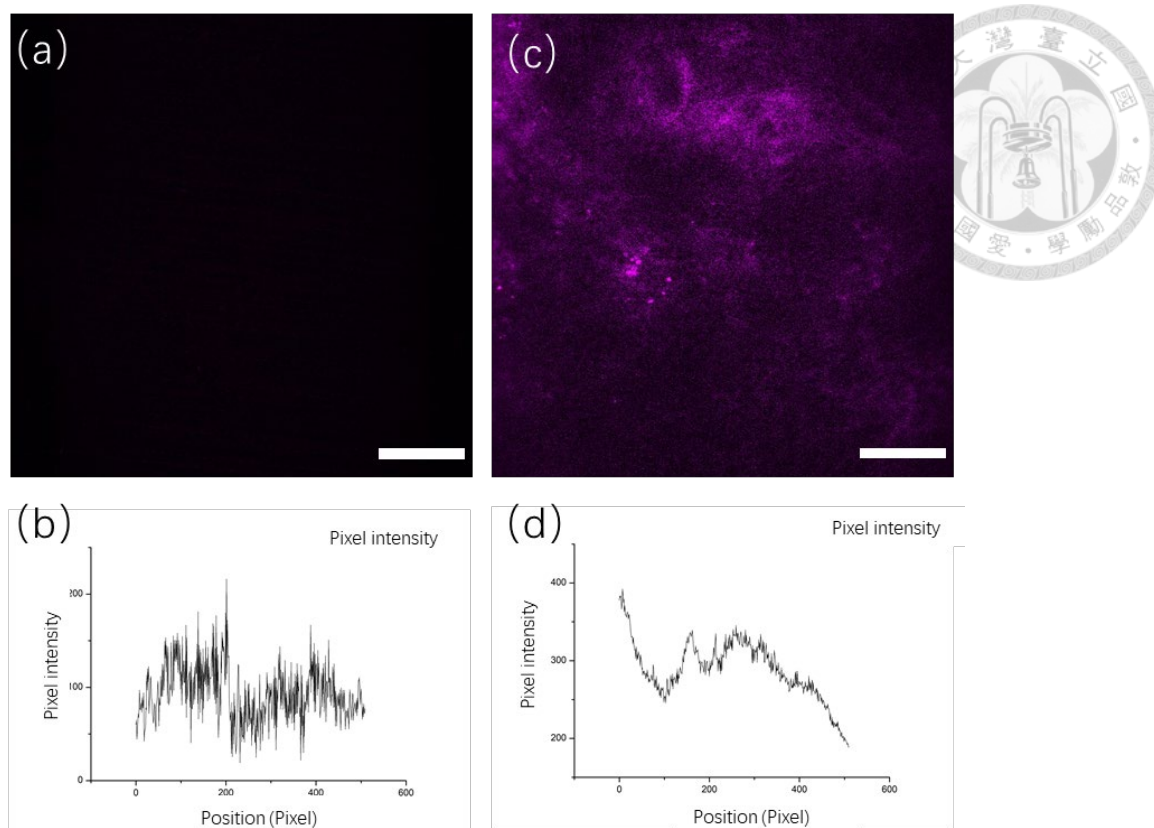
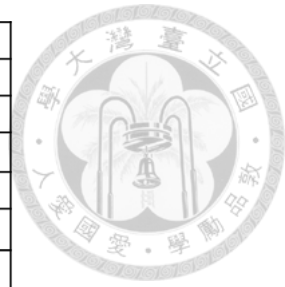


Fig. 5.2.2.5 THG images and its pixel intensity changing. (a) The HGM image of normal connective tissues without SHG signal in normal volunteer. (b) The pixel intensity of THG signal of normal connective tissues in image(a). (c) The connective tissue of HGM image of AK patient 00 without SHG signal. (d) The pixel intensity of THG signal of AK patient 00's connective tissues in image (c). Scale bar=50  $\mu\text{m}$ .

While in normal connective tissue (Fig. 5.2.4.5 (b)), the average THG pixel intensity is 93.26, the average THG pixel intensity of AK patient 00's connective tissues is 288.73, which is 3.09 times higher. This indicates that the intensity of THG signal of connective tissues of AK patient 00 is significantly enhanced due to increased deposition of elastin materials. HGM thus suggests the solar elastosis in AK patient 00.

From the above, the morphology of epidermis in AK is legible in HGM images and high consistency between H&E and HGM images can be found. Furthermore, we list the evaluation results in Table 5.2.2.6.



		H&E	HGM
Stratum corneum	Parakeratosis	+	+
	Hyperkeratosis	+	+
Stratum spinosum	Irregular acanthosis	+	+
	Abnormal architecture	+	+
	Pleomorphisms of cells and nuclei	+	+
Stratum basale	Crowding of keratinocytes	+	+
	Abnormal architecture	+	+
	Pleomorphisms of abnormal cells and nuclei	+	+
Dermis	solar elastosis	+	+

Table 5.2.2.6 The evaluation results of H&E and HGM for AK patient 00. “+” represents that this feature can be recognized. “-” represents that this feature does not exist. “NA” represents that this feature is uncertain to recognize.

H&E sections are always viewed in the transverse direction. In another AK lesion sample taken from the left cheek of AK patient 00, we took the *ex vivo* HGM images of the fresh whole mount tissue sample with virtual transverse sectioning. This result in the same viewing direction for the stratum basale between HGM image (Fig. 5.2.2.7 (a)) and H&E histopathology image (Fig. 5.2.2.7 (b)).

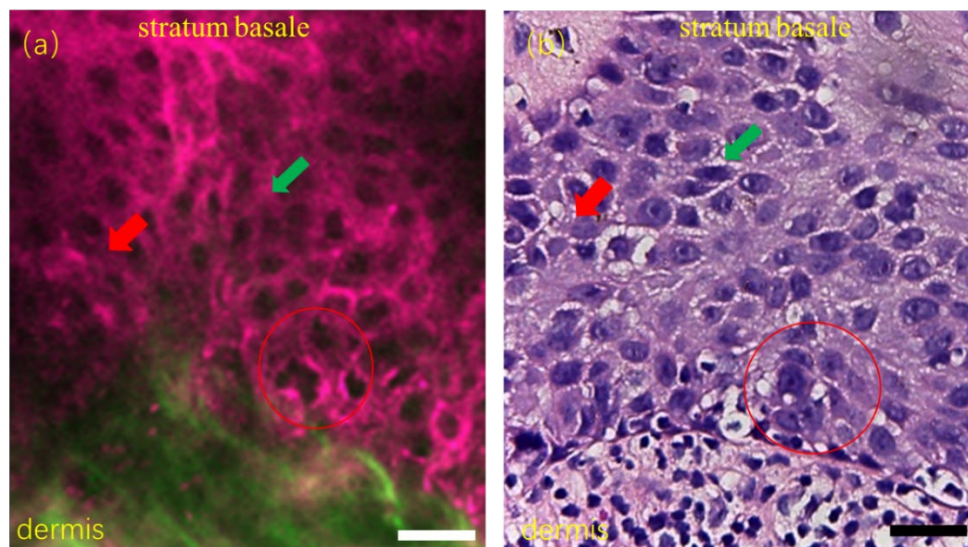


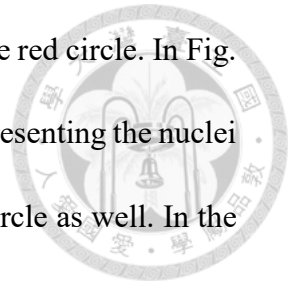
Fig. 5.2.2.7 The transverse sectioned images of the stratum basale of AK patient 00 in the same left cheek lesion. (a) The labeled image is HGM of AK. (b) The labeled image is the conventional histopathology of AK. In the red circle (a), the black hole representing the nuclei of the basal cell takes up the majority of the cell volume. In the red circle (b), the darker hole representing the nuclei of the basal cell takes up the majority of the cell volume. In the red arrows, cells are crowding to each other. In the green arrows, these cells are bending and slender. Scale bar=10  $\mu$ m.

In Fig. 5.2.2.7, we can also see the consistent morphology between HGM and traditional H&E images. In Fig. 5.2.2.7 (a), the labeled image of HGM shows that the



---

dark basal nuclei take up the majority of the cell volume shown in the red circle. In Fig. 5.2.2.7 (b), the labeled image of H&E shows that the darker hole representing the nuclei of the basal cell take up the majority of the cell volume in the red circle as well. In the red arrows, cells are crowding to each other. These cells are bending and slender (green arrows). Both imaging modality indicate consistent architectural disarray and cytologic atypia with large and pleomorphic nuclei and cells.



### 5.2.3 Result of the AK Patient 01

Following the evaluation standard in Table 2.3.2.1, Fig. 5.2.3.1 exemplifies the H&E histopathology of the AK patient 01 in a transverse section, whereas Fig. 5.2.3.2 illustrates representative *in vivo* HGM images of the same AK lesion taken before its biopsy examination.

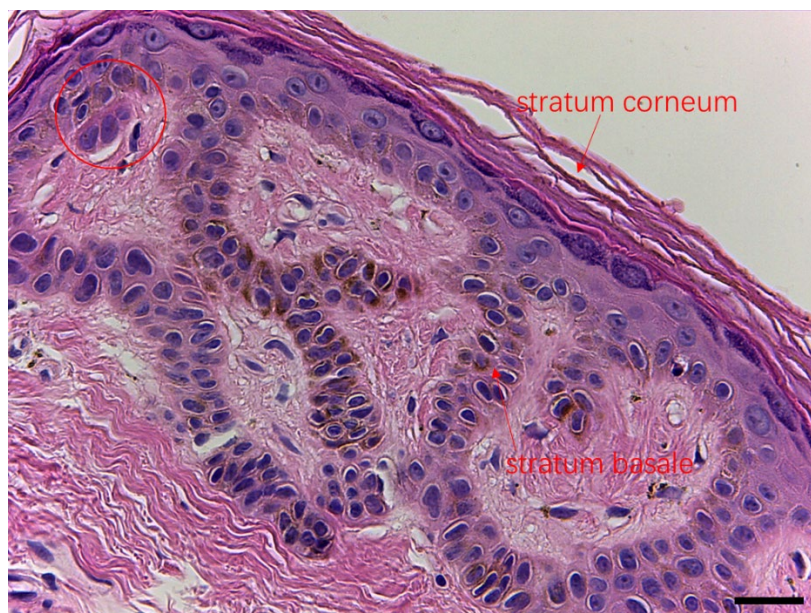


Fig. 5.2.3.1 A transverse histopathology section of the AK patient 01 on the skull. In the stratum corneum, it shows hyperkeratosis. In the stratum basale, it shows architectural disarray, crowding keratinocytes and cytologic atypia with large and pleomorphic nuclei and cells (red circle). Scale bar=10  $\mu$ m.

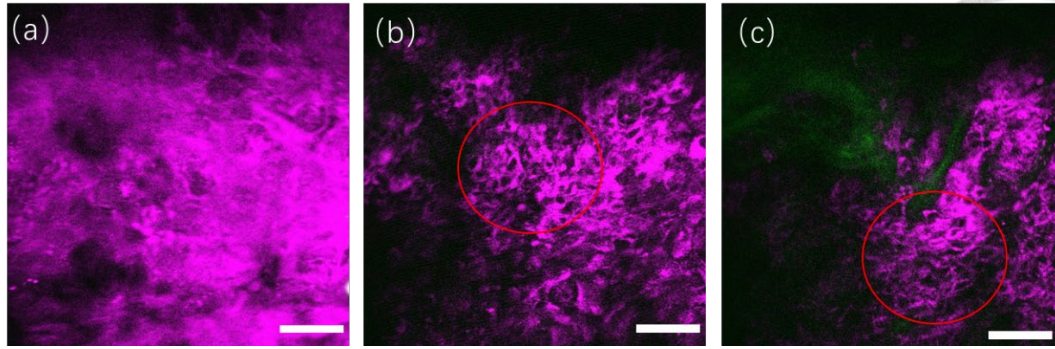
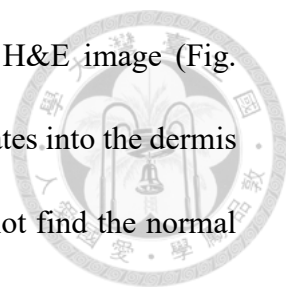


Fig. 5.2.3.2 *In vivo* HGM *en face* virtual sectioned images of AK patient 01 on the skull. [(a) to (c)] A representative series of *in vivo* HGM images taken at different depths relative to the surface in AK patient 01. (a) Stratum corneum. (b) Stratum basale. (c) Stratum basale. In the red circles (b) and (c), it shows that nuclei take up the majority of the cell volume. Scale bar=50  $\mu\text{m}$ .

From the H&E histopathology image of AK patient 01 (Fig. 5.2.3.1) with the evaluation standard and the normal H&E image (Fig. 2.2.2.2(b)), it shows hyperkeratosis due to the abnormal thickness in the stratum corneum. The stratum basale shows architectural disarray, crowding keratinocytes and cytologic atypia with large and pleomorphic nuclei and cells. In the red circle (Fig. 5.2.3.1), melanin deposition can be found and it indicated pigmented type AK. While in the *in vivo* HGM image (Fig. 5.2.3.2(a)), there are no nuclei in the stratum corneum and the thickness of the stratum corneum is 31.2  $\mu\text{m}$  (52 pictures). HGM thus suggests hyperkeratosis but not parakeratosis which is the same result as Fig. 5.2.3.1.

In the H&E image (Fig. 5.2.3.1), the stratum basale shows architectural disarray, crowding keratinocytes and cytologic atypia with large and pleomorphic nuclei and cells. In the HGM image of AK patient 01 (Fig. 5.2.3.2(b)), it also shows architectural disarray in comparison with the normal HGM image (Fig. 5.2.1(e)). Moreover, the basal cells are all pleomorphic and in different sizes. The basal cells of the H&E image are all with pathological abnormality and we cannot find the normal basal cells. In the red circle in HGM images (Fig. 5.2.3.2(b)), it shows that nuclei take up the majority of the

cell volume which is the same phenomenon in the red circle in H&E image (Fig. 5.2.3.1). In HGM image (Fig. 5.2.3.2 (c)), the stratum basale penetrates into the dermis which is the same in H&E image (Fig. 5.2.3.1). Similarly, we cannot find the normal basal cells in HGM images as well (Fig. 5.2.3.3(c)).



In the dermis of H&E image (Fig. 5.2.3.1) the connective tissues are pink. It means normal. Due to the limitation of HGM images, we cannot find the HGM image which only contains connective tissue without basal cells. Therefore, for AK patient 01 we cannot analyze the intensity of THG signal to recognize the existing of solar elastosis.

Form above, the morphology of stratum corneum and stratum basale in AK of HGM images is legible with high consistency between H&E and HGM images. Moreover, the morphology of stratum corneum and stratum basale is the most important judgement condition for the diagnosis of pathologist. The basal cells are all pathological abnormal and we cannot find the normal basal cells both in H&E and HGM images. This patient belongs to the severe type (AK III). In addition, we list the evaluation results in Table 5.2.3.3.

		H&E	HGM
Stratum corneum	Parakeratosis	-	-
	Hyperkeratosis	+	+
Stratum spinosum	Irregular acanthosis	-	NA
	Abnormal architecture	+	NA
	Pleomorphisms of cells and nuclei	+	NA
Stratum basale	Crowding of keratinocytes	+	+
	Abnormal architecture	+	+
	Pleomorphisms of abnormal cells and nuclei	+	+
Dermis	solar elastosis	-	NA

Table 5.2.3.3 The evaluation results of H&E and HGM for AK patient 01. “+” represents that this feature can be recognized. “-” represents that this feature does not exist. “NA” represents that this feature is uncertain to recognize.

We cannot take the available HGM images of the stratum spinosum due to the time limitation and the shaking of patient. For the pigmented type, the THG signal of

---

pigmented basal cells should be stronger than unpigmented basal cells. But the THG intensity of unpigmented basal cells is already in saturation. So, in our specific PMT condition, HGM images cannot distinguish pigmented type from unpigmented AK. For future improvement, modification of PMT voltage during image acquisition might be necessary.

## 5.2.4 Result of the AK Patients 03 and 04

The results of AK patient 03 and 04 are shown in Fig. 5.2.4.1, Fig. 5.2.4.2, Fig. 5.2.4.3 and Fig. 5.2.4.4. Fig. 5.2.4.1 shows the H&E images of AK patient 03 and Fig. 5.2.4.2 shows the *in vivo* HGM images of AK patient 03. Fig. 5.2.4.3 shows the H&E images of AK patient 04 and Fig. 5.2.4.3 shows the *in vivo* HGM images of AK patient 04.

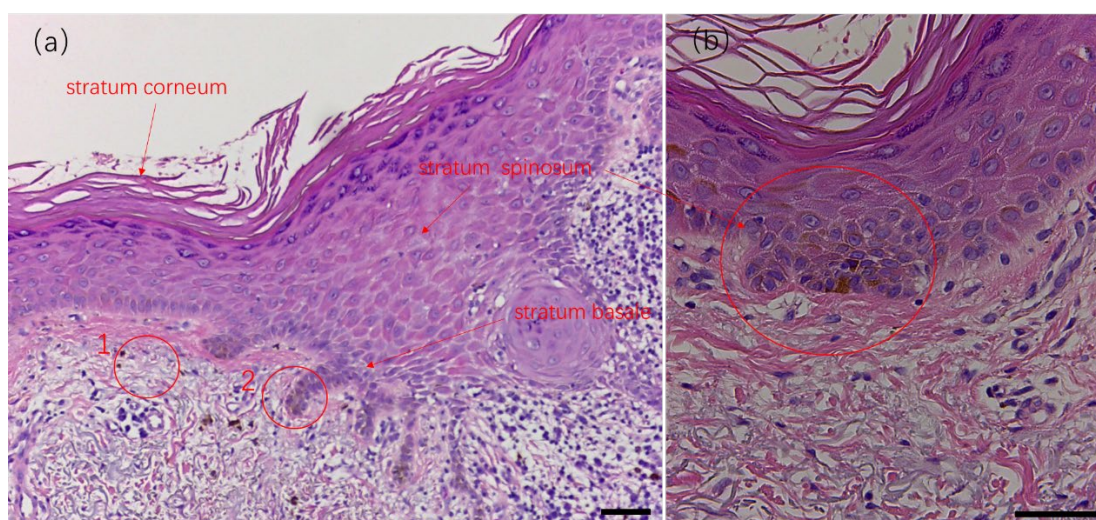


Fig. 5.2.4.1 Two transverse histopathology sections of the AK patient 03 in the same lesion of cheek. (a) In the stratum corneum, hyperkeratosis is obvious to see and there is no parakeratosis. The thickness of the stratum corneum is thicker than the normal one. In the stratum spinosum, cell atypia is not obvious to see and it shows normal architecture. Irregular acanthosis exists in the stratum spinosum. In the stratum basale, abnormal architecture is obvious. The cells crowding to each other are in different sizes and shapes. In the circle 1, solar elastosis happens in the dermis. The connective tissues change into purple while the normal connective tissues are pink in H&E image.

In the circle 2, the basal cells are pigmented. (b) In the red circle, cell atypia is obvious in the stratum spinosum. Scale bar=10  $\mu$ m.

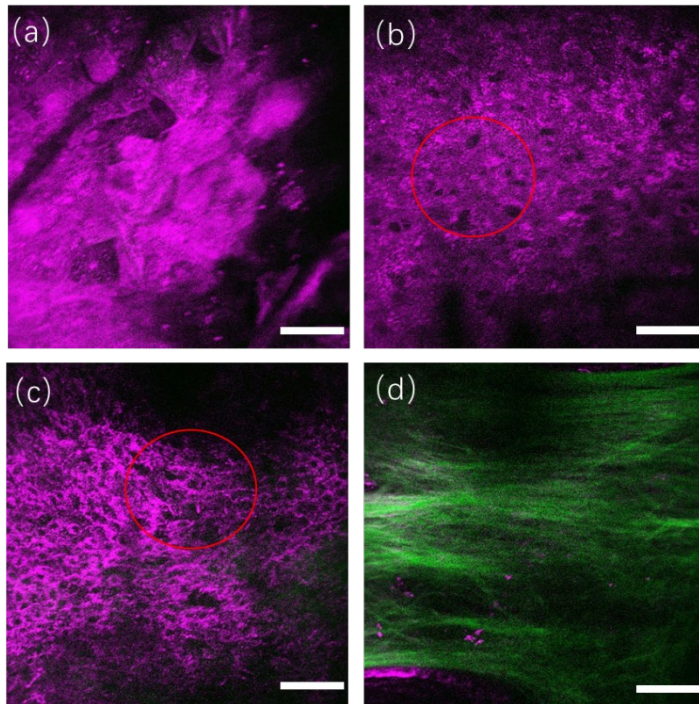


Fig. 5.2.4.2 Actinic keratosis [(a) to (d)] A representative series of *in vivo* HGM *en face* sectioned images at different depths relative to the surface in AK patient 03. The lesion is on the cheek. (a) Stratum corneum. There is hyperkeratosis and not parakeratosis. (b) Stratum spinosum. Stratum spinosum shows architectural disarray and cytologic atypia with large and pleomorphic nuclei and cells in the red circle. (c) Stratum basale. The stratum basale shows architectural disarray, crowding keratinocytes and cytologic atypia with large and pleomorphic nuclei and cells. (d) Dermis. Scale bar=50  $\mu$ m.

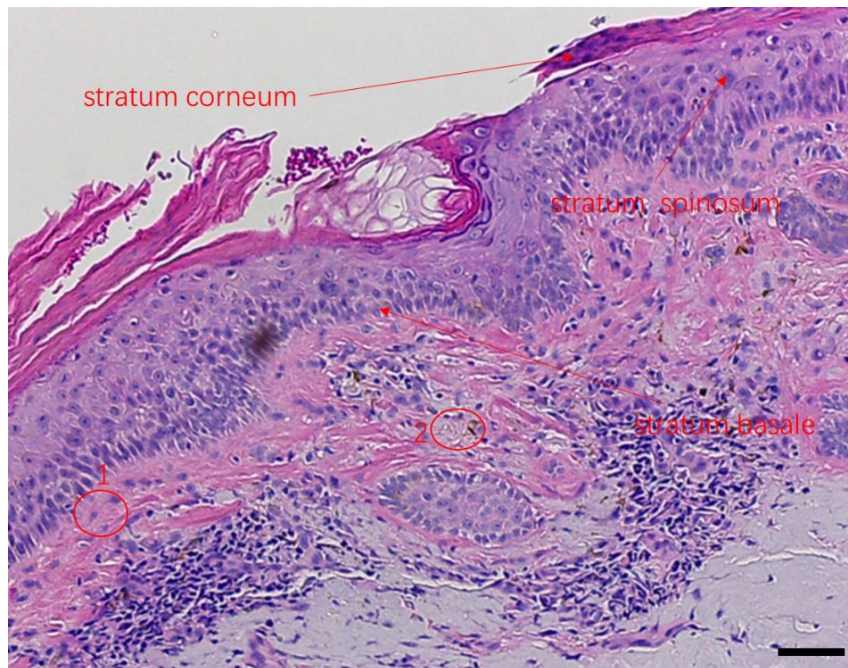


Fig. 5.2.4.3 A transverse histopathology section of the AK patient 04 on the cheek. In the stratum corneum, hyperkeratosis is obvious to see and there is parakeratosis in label. The thickness of the stratum corneum is thicker than the normal one. In the stratum spinosum, these cells are all in different sizes and it indicted abnormal architecture.

Irregular acanthosis is in the stratum spinosum. In the stratum basale, abnormal architecture is obvious. The cells crowding to each other are in different sizes and shapes. In the circle 1, connective tissues are normal and pink. In the circle 2, solar elastosis happens in the dermis. The connective tissues change into purple amorphous appearance. Scale bar=10  $\mu\text{m}$ .

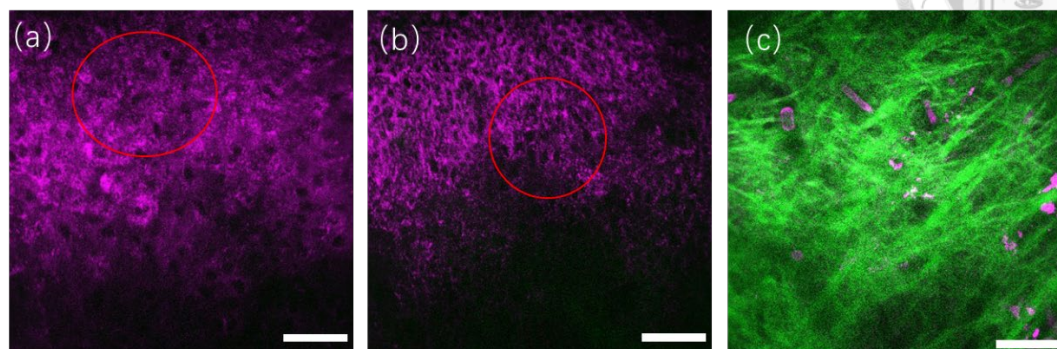


Fig. 5.2.4.4 Actinic keratosis [(a) to (c)] A representative series of *in vivo* HGM *en face* sectioned images at different depths relative to the surface in AK patient 04. The lesion is on the cheek. (a) Stratum spinosum. Stratum spinosum shows architectural disarray and cytologic atypia with large and pleomorphic nuclei and cells in the red circles. (b) Stratum basale. The stratum basale shows architectural disarray, crowding keratinocytes and cytologic atypia with large and pleomorphic nuclei and cells. (c) Dermis. Scale bar=50  $\mu\text{m}$ .

The H&E & HGM results of AK patients 03 and 04 are similar. In H&E images of AK patient 03 (Fig. 5.2.4.1) and AK patient 04 (Fig. 5.2.4.3), the thickness of the stratum corneum is thicker than normal stratum corneum shown in normal H&E image (Fig. 2.3.2.2(b)). It's obvious to show hyperkeratosis in AK patient 03 and 04. The nuclei are still in the stratum corneum in H&E images of AK patient 04 (Fig. 5.2.4.3). So, AK patient 04 is parakeratosis. In HGM image of AK patient 03 (Fig. 5.2.4.2(a)), the stratum corneum is 12.6  $\mu\text{m}$  thick (21 pictures) which is more than 11  $\mu\text{m}$ . So, HGM suggests hyperkeratosis for AK patient 03. However, for AK patient 04 there are no available HGM images of the stratum corneum due to time limitation and shaking of the patient. Therefore, we cannot estimate the thickness of the stratum corneum for AK patient 04 in HGM to recognize the hyperkeratosis.

In H&E images of AK patient 03 (Fig. 5.2.4.1 (b)) and AK patient 04 (Fig. 5.2.4.3), the stratum spinosum shows architectural disarray and cytologic atypia with large and

---

pleomorphic nuclei and cells. The thickness of the stratum spinosum is thicker than normal one. It is irregular acanthosis. AK patient 03 is shown in Fig. 5.2.4.1 (a). In the HGM image of AK patient 03 (Fig. 5.2.4.2(b)), the thickness of the stratum spinosum is 16.8  $\mu\text{m}$  (28 pictures). In the HGM image of AK patient 04 (Fig. 5.2.4.4(a)), the thickness of the stratum spinosum is 19.2  $\mu\text{m}$  (32 pictures). The thickness of AK patient 03 of the stratum spinosum is less than the normal one (19  $\mu\text{m}$ ) while the thickness of AK patient 04 of the stratum spinosum is more than the normal one (19  $\mu\text{m}$ ). HGM thus suggests irregular acanthosis in AK patient 04 but not in AK patient 03. The possible reason is that stratum spinosum of AK patient 03 is not thick everywhere and the HGM sampled in normal position. In Fig. 5.2.4.2(b) and Fig. 5.2.4.4(a), it also shows architectural disarray and cytologic atypia with large and pleomorphic nuclei and cells, different from normal cells in normal HGM images (Fig. 5.2.1(d)). HGM thus suggests abnormal architecture and pleomorphism of cells and nuclei in the stratum spinosum.

In H&E images of AK patient 03 (Fig. 5.2.4.1) and AK patient 04 (Fig. 5.2.4.3), the stratum basale still shows architectural disarray and cytologic atypia with large and pleomorphic nuclei and cells. These cells are all closely crowding to each other, different from the normal H&E image (Fig. 2.3.2.2(b)). Especially in Fig. 5.2.4.1, the circle 1 shows the pigmented type. In HGM images of AK patient 03 (Fig. 5.2.4.2(c)) and AK patient 04 (Fig. 5.2.4.4(b)), the stratum basale shows architectural disarray, different from the normal one in normal HGM image (Fig. 5.2.1(f)). Normal basal cells in Fig. 5.2.1(f) are oval rather than bending and slender in Fig. 5.2.4.2(c) and Fig.

5.2.4.4(b). Moreover, basal cells in Fig. 5.2.4.2(c) and Fig. 5.2.4.4(b) are more crowding to each other than cells in Fig. 5.2.1(f).

In the circle 1 of H&E image (Fig. 5.2.4.3), connective tissues are normal and pink. In the circle 2 of Fig. 5.2.4.3 and in the circle 1 of Fig. 5.2.4.1, solar elastosis happens in the dermis and the color of connective tissues is purple. Same as above, to control the same layer with normal comparison, the HGM images of AK patients 03 and AK patient 04 are the 10<sup>th</sup> layer after the cell structures are disappeared absolutely. We show the result of increased THG pixel intensity in *in vivo* HGM images in Fig. 5.2.4.5. Fig. 5.2.4.5 (a) shows the THG image of normal connective tissue without SHG signal and Fig. 5.2.4.5 (b) shows the pixel intensity of THG signal of normal connective tissue. Fig. 5.2.4.5 (c) shows the connective tissue of THG image of AK patient 03 without SHG signal and Fig. 5.2.4.5 (d) shows the pixel intensity of THG signal of the connective tissue of AK patient 03. Fig. 5.2.4.5 (e) shows the connective tissue of THG image of AK patient 04 without SHG signal and Fig. 5.2.4.5 (f) shows the pixel intensity of THG signal of the connective tissue of AK patient 04.

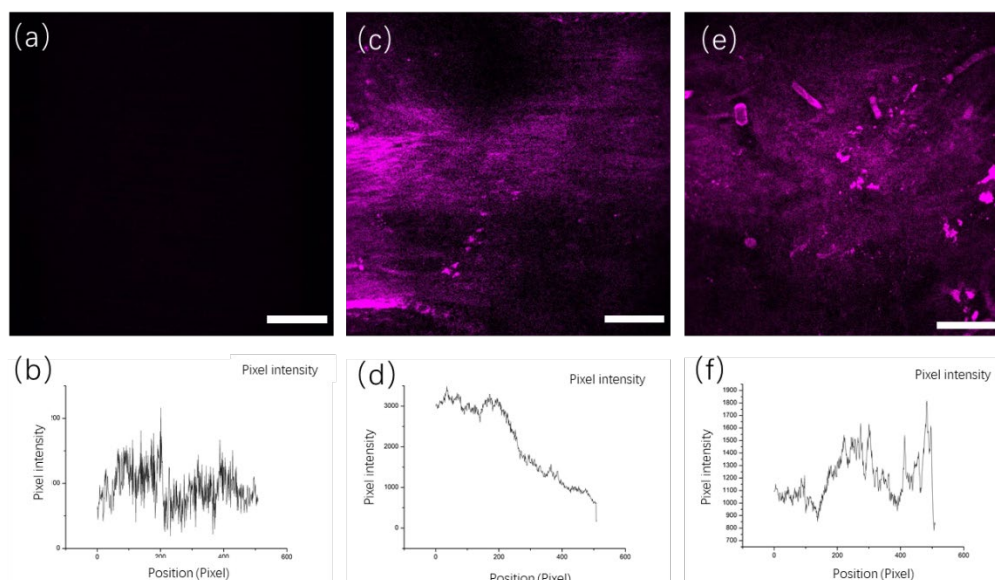




Fig. 5.2.4.5 THG images without SHG signal and its pixel intensity changing. (a) The THG image of normal connective tissue without SHG signal in normal volunteer. (b) The pixel intensity of THG signal of normal connective tissue in the image (a). (c) The connective tissue of THG image of AK patient 03 without SHG signal. (d) The pixel intensity of THG signal of AK patient 03's connective tissue in image(c). (e) The connective tissue of THG image of AK patient 04 without SHG signal. (f) The pixel intensity of THG signal of AK patient 04's connective tissue in the image (e). Scale bar=50  $\mu\text{m}$ .

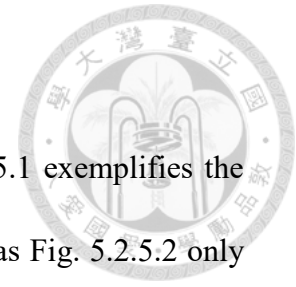
While in normal connective tissue (Fig. 5.2.4.5 (b)), the average THG pixel intensity of normal connective tissue is 93.26, the average THG pixel intensity of AK patient 03's connective tissues is 2115.42, which is 22.68 times higher. Meanwhile the average THG pixel intensity of AK patient 04's connective tissues is 1203.14, which is 12.9 times higher than normal value. This indicates that the intensities of THG signal of connective tissues of AK patient 03 and AK patient 04 are significantly enhanced due to increased deposition of elastin materials. HGM thus suggests the solar elastosis in AK patients 03 and 04.

From the above, the morphology of epidermis in AK is legible in HGM images and high consistency between H&E and HGM images can be found. Furthermore, we list the evaluation results in Table 5.2.4.6.

		AK 03H&E	AK 03HGM	AK 04H&E	AK 04HGM
Stratum corneum	Parakeratosis	-	-	+	NA
	Hyperkeratosis	+	+	+	NA
Stratum spinosum	Irregular acanthosis	+	-	+	+
	Abnormal architecture	+	+	+	+
	Pleomorphisms of cells and nuclei	+	+	+	+
Stratum basale	Crowding of keratinocytes	+	+	+	+
	Abnormal architecture	+	+	+	+
	Pleomorphisms of abnormal cells and nuclei	+	+	+	+
dermis	solar elastosis	+	+	+	+

Table 5.2.4.6 The evaluation results of H&E and HGM for AK patient 03 and 04. "+" represents that this feature can be recognized. "-" represents that this feature does not exist. "NA" represents that this feature is uncertain to recognize.

## 5.2.5 Result of the AK Patient 02



Following the evaluation standard in Table 2.3.2.1, Fig. 5.2.5.1 exemplifies the histopathology of the AK patient 02 in a transverse section, whereas Fig. 5.2.5.2 only illustrates representative *in vivo* HGM images of the same AK lesion in the stratum spinosum and the stratum basale. The HGM images of the stratum corneum are not available due to the limitation of time and the shaking of patient. The HGM images of the stratum spinosum are not continuous in a stack so that we can not calculate the thickness of the stratum spinosum.

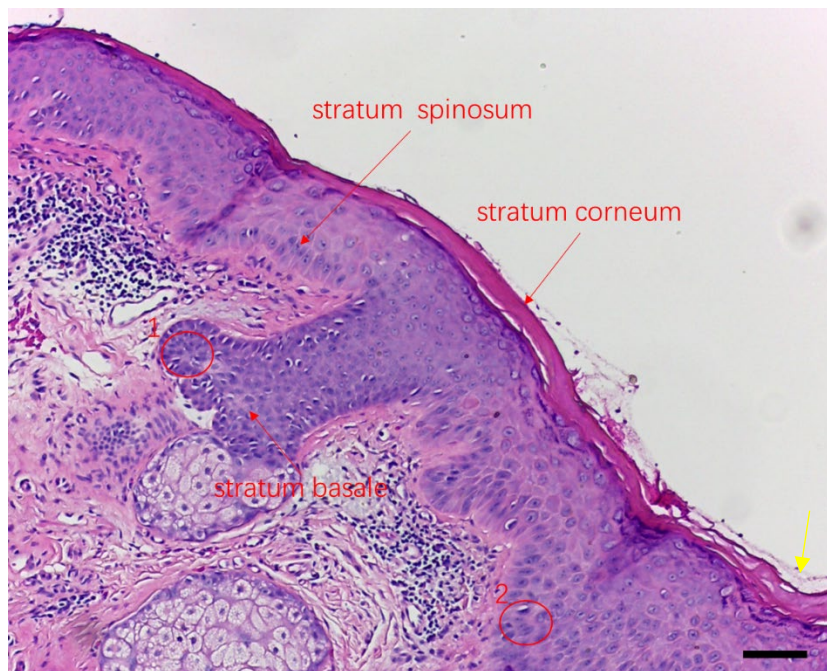


Fig. 5.2.5.1 A transverse histopathology section of the AK patient 02 on the cheek. In the stratum corneum, it is normal. In the stratum spinosum, it is normal as well. In the stratum basale, the cells crowding to each other are in different sizes and shapes in the circle 1. In the circle 2, basal cells are normal. Scale bar=10  $\mu$ m.

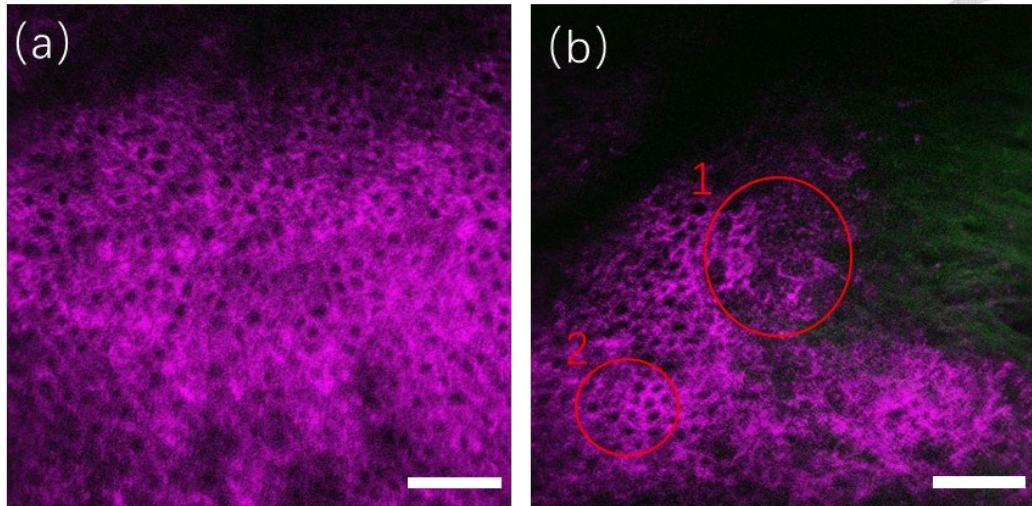


Fig. 5.2.5.2 Actinic keratoses [(a) and (b)] A representative series of *in vivo* HGM *en face* sectioned images at different depths relative to the surface in AK patient 02. The lesion is on the cheek. (a) Stratum spinosum. The stratum spinosum is normal. (b) Stratum basale. The stratum basale shows crowding keratinocytes and cytologic atypia with pleomorphic cells in the circle 1. In the circle 2, the basal cells are normal. Scale bar=50 $\mu$ m.

In the H&E image of AK patient 02 (Fig. 5.2.5.1), the stratum corneum is almost normal and the thickness of the stratum corneum only gets thicker a little in the yellow arrow. In the stratum spinosum, cells are normal as well. In the stratum basale, basal cells crowding to each other are in different sizes and shapes in the circle 1. In the circle 2, basal cells are normal. In HGM images of AK patient 02 (Fig. 5.2.5.2), the stratum spinosum is normal. In the stratum basale, it shows crowding keratinocytes and cytologic atypia with pleomorphic cells in the circle 1. In the circle 2, the basal cells are normal. According to H&E, AK patient 02 is in mild grade of AK (AK I) and pathological changes are only in the stratum basale. In the H&E image (Fig. 5.2.5.1), it shows normal in the dermis because connective tissues are pink. However, the HGM images of AK patients 02 is the 5<sup>th</sup> layer after the cell structures are disappeared absolutely due to the shaking of patient. Therefore, to control the same conditions we also use the normal image of 5<sup>th</sup> layer after the cell structures are disappeared absolutely. Same as above, with the same comparison standard we show the result of increased

THG pixel intensity in *in vivo* HGM images in Fig. 5.2.5.3. Fig. 5.2.5.3 (a) shows the THG image of normal connective tissue without SHG signal and Fig. 5.2.5.3 (b) shows the pixel intensity of THG signal of normal connective tissue. Fig. 5.2.5.3 (c) shows the connective tissue of THG image of AK patient 02 without SHG signal and Fig. 5.2.5.3 (d) shows the pixel intensity of THG signal of the connective tissue of AK patient 02.

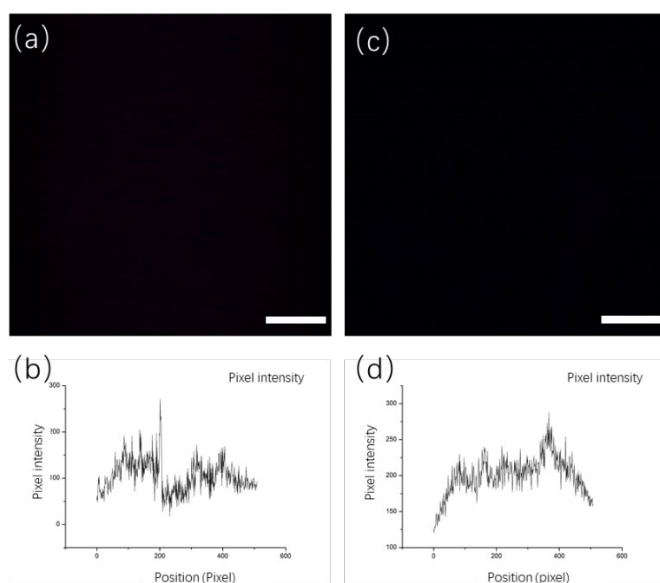


Fig. 5.2.5.3 THG images without SHG signal and its pixel intensity changing. (a) The HGM image of normal connective tissue without SHG signal in normal volunteer. (b) The pixel intensity of THG signal of normal connective tissue in image(a). (c) The connective tissue of HGM image of AK patient 02 without SHG signal. (d) The pixel intensity of THG signal of AK patient 02's connective tissue in image(c). Scale bar=50  $\mu\text{m}$ .

While in normal connective tissue (Fig. 5.2.4.5 (b)), the average THG pixel intensity is 105.35, the average THG pixel intensity of AK patient 02's connective tissues is 199.79, which is only 1.89 times higher. In comparison with other cases and normal values, the pixel intensity of THG signal of connective tissues of AK patient 02 is much lower. Therefore, this indicates that the pixel intensity of THG signal of connective tissues of AK patient 02 is not enhanced obviously. HGM thus suggests normal connective tissue for AK patient 02.

From above, we list the evaluation results in Table 5.2.4.4.

		H&E	HGM
Stratum corneum	Parakeratosis	-	-
	Hyperkeratosis	+	NA
Stratum spinosum	Irregular acanthosis	+	NA
	Abnormal architecture	-	-
	Pleomorphisms of cells and nuclei	-	-
Stratum basale	Crowding of keratinocytes	+	+
	Abnormal architecture	+	+
	Pleomorphisms of abnormal cells and nuclei	+	+
Dermis	solar elastosis	-	-



Table 5.2.5.4 The evaluation results of H&E and HGM for AK patient 02. “+” represents that this feature can be recognized. “-” represents that this feature does not exist. “NA” represents that this feature is uncertain to recognize.

After treatment of cryotherapy, due to contingencies there is only one after-treatment patient (AK patient 02). We took HGM *en face* virtual sectioned images in the same location (before treatment HGM, treatment) of AK patient 02 shown in Fig. 5.2.5.5.

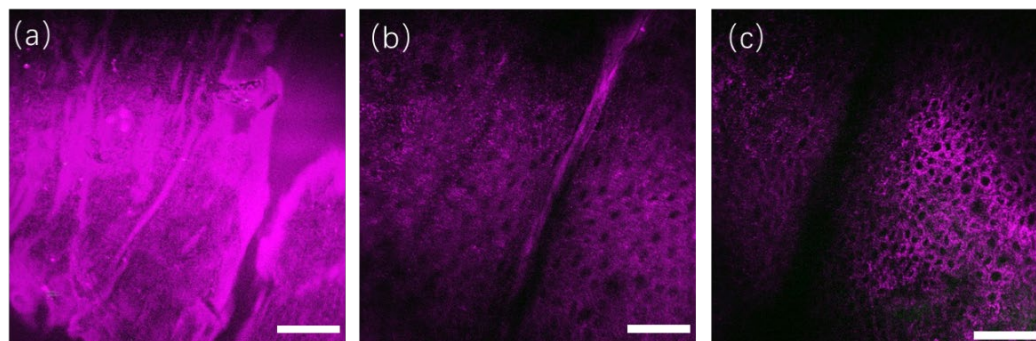


Fig. 5.2.5.5 *En face* sectioned HGM images of AK patient 02 in the same location after two months. [(a) to (c)] The lesion is on the cheek. (a) Stratum corneum. It is normal. (b) Stratum spinosum. It is normal. (c) Stratum basale. It is normal. Scale bar=50  $\mu\text{m}$ .

From after-treatment HGM images of AK patient 02 (Fig. 5.2.5.5) with the evaluation standard and normal H&E image (Fig. 2.3.2.2 (b)), the stratum corneum shows normal (Fig. 5.2.5.5 (a)). The thickness of the stratum corneum is 7.2  $\mu\text{m}$  (12 pictures), which is less than 11  $\mu\text{m}$  and normal. In in Fig. 5.2.5.5 (b) and (c), the stratum spinosum and the stratum basale show architectural order and cells are oval. The thickness of the stratum spinosum is 9  $\mu\text{m}$  (15pictures), which is normal as well. No

H&E biopsy was taken for comparison. Usually no biopsy examination is allowed after treatment.



## 5.2.6 Summary

The Roewert-Huber histological classification system grades AK lesions based on the extent of epidermal atypical keratinocytes (AK I–III).<sup>[47]</sup> AK III is the most severe. AK II is moderate. AK I is mild. So, we show a summary table for 5 diagnosis cases.

(The comparison of H&E and HGM images in Table 5.2.6.1)

		AK 00 H&E	AK 00 HGM	AK 01 H&E	AK 01 HGM	AK 02 H&E	AK 02 HGM	AK 03 H&E	AK 03HGM	AK 04H&E	AK 04HGM
Stratum corneum	Parakeratosis	+	+	-	-	-	-	-	-	+	NA
	Hyperkeratosis	+	+	+	+	+	NA	+	+	+	NA
Stratum spinosum	Irregular acanthosis	+	+	-	NA	+	NA	+	-	+	+
	Abnormal architecture	+	+	+	NA	-	-	+	+	+	+
	Pleomorphisms of cells and nuclei	+	+	+	NA	-	-	+	+	+	+
Stratum basale	Crowding of keratinocytes	+	+	+	+	+	+	+	+	+	+
	Abnormal architecture	+	+	+	+	+	+	+	+	+	+
	Pleomorphisms of abnormal cells and nuclei	+	+	+	+	+	+	+	+	+	+
dermis	solar elastosis	+	+	-	NA	-	-	+	+	+	+
diagnosis		AK grade III	AK grade III	AK grade II	AK grade II	AK grade I	AK grade I	AK grade II	AK grade II	AK grade II	AK grade II

Table 5.2.6.1 Summary of diagnosis results of 5 patients. “+” represents that this feature can be recognized. “-” represents that this feature does not exist. “NA” represents that this feature is uncertain to recognize. AK grade represents the severity of AK. AK grade III represents serious AK. AK grade II represents middle AK. AK grade I represents mild AK.

From the Table 5.2.6.1, it shows the high consistency between H&E and HGM images. The sensitivity of diagnosis for AK is 100% although we only have 5 cases. Moreover, the evaluation of severity for AK is still accurate. AK patient 00 is predicated AK grade III (severe) by H&E because pathological changes happened in the whole epidermis and the morphology of epidermis of AK patient 00 is pathologically severe. The evaluation of severity for AK by HGM is also AK grade III (severe) because

---

pathological changes happened in whole epidermis and the morphology of epidermis of AK patient 00 is pathologically severe. For AK patients 01, 03 and 04, pathological changes did not happen in the whole epidermis and we can find the normal parts in both H&E and HGM images. Therefore, the evaluations of severity for AK patients 01, 03 and 04 are AK grade II (moderate). For AK patients 02, the pathological changes only happened in the stratum basale in both H&E and HGM images. The evaluation of severity for AK patients 01 is AK grade I (mild).

### 5.3 Discussion

With the development of AK, it was reported that melanocytes were more active than normal situation due to proliferation and differentiation in the epidermis<sup>[48][49]</sup>, which caused the increased number of dendritic structures. But it cannot be recognized in H&E images except under specific staining. In our HGM results, we almost see dendritic-like cells in all cases except AK patient 02. It shows in Fig 5.3.1. Moreover, we list the distribution of THG dendritic-cell-like signals in 5 patients shown in Table 5.3.2.

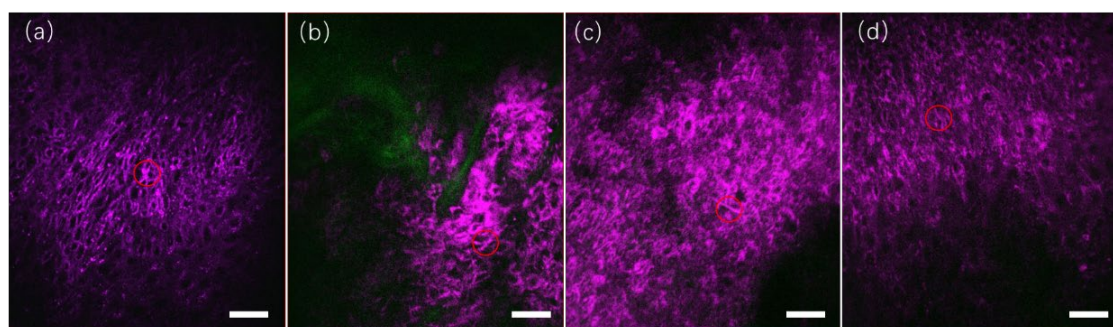
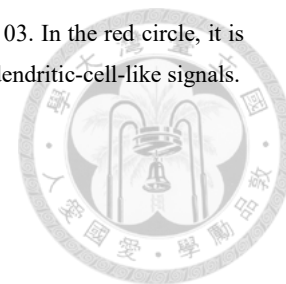


Fig. 5.3.1 *En face* sectioned *ex vivo* and *in vivo* HGM images of AK patients in the stratum basale. (a) The stratum basale of AK patient 00. In the red circle, it shows dendritic-cell-like signals. (b) The stratum basale of AK patient

01. In the red circle, it is dendritic-cell-like signals. (c) The stratum basale of AK patient 03. In the red circle, it is dendritic-cell-like signals. (a) The stratum basale of AK patient 04. In the red circle, it is dendritic-cell-like signals.



Case	Sampling	THG	Severity
AK patient 00	Ex vivo	+	AK grade III
AK patient 01	In vivo	+	AK grade II
AK patient 02	In vivo	-	AK grade I
AK patient 03	In vivo	+	AK grade II
AK patient 04	In vivo	+	AK grade II

Table 5.3.2 The basal distribution of THG-bright dendritic-cell-like signals in 5 AK patients. “+” represents that this feature can be recognized. “-” represents that this feature does not exist. AK grade represents the severity of AK. AK grade I represents mild AK. AK grade II represents moderate AK. AK grade III represents severe AK.

From Table 5.3.2, the dendritic structures are related to the severity of AK. The AK patient 02 is the only one without dendritic structures and the patient is happened to be the only in mild AK (AK grade I). To prove the result, more patients should be collected in future research.

In current situation of non-invasive way for AK diagnosis, OCT and RCM have made progress.

For OCT, images obtained in 2014 using a “VivoSight” OCT system from Michelson Diagnostics, UK with a resolution of  $<5 \mu\text{m}$  axial and  $<7.5 \mu\text{m}$  lateral and a scan area of  $6 \times 6 \text{ mm}$ . The penetration depth of system was 1-2 mm. The lateral resolution is  $7.5 \mu\text{m}$  lateral and vertical resolution was  $10 \mu\text{m}$ . Their images are shown in Fig. 5.3.3.<sup>[12]</sup> From Fig. 5.3.3, OCT could not recognize the morphology and it distinguished AK from normal skin only dependent on the thickness of epidermis. Therefore, the main work of OCT for AK was measuring the thickness of epidermis and calculating the sensitivity of OCT by kappa analysis.



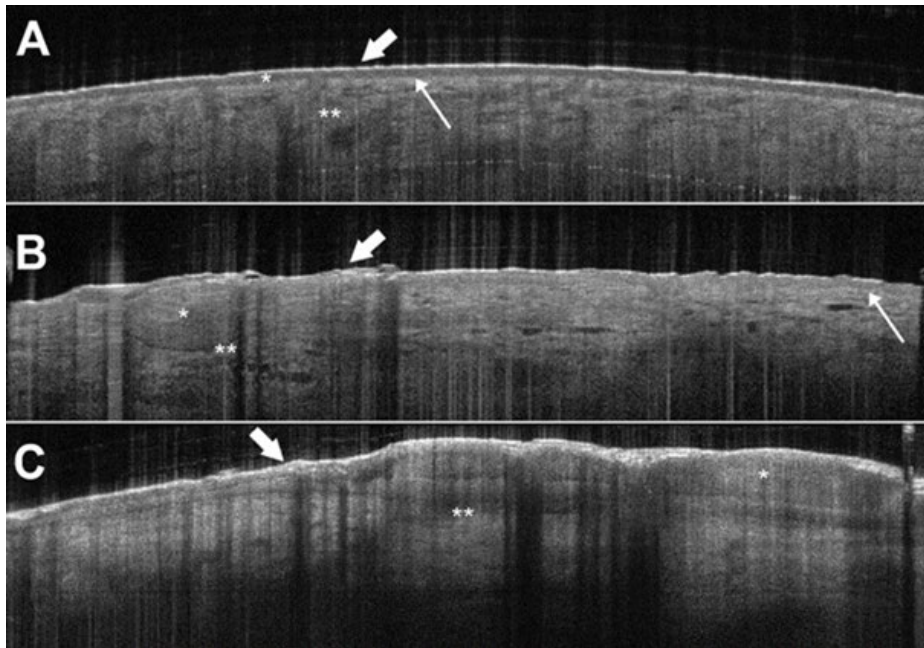
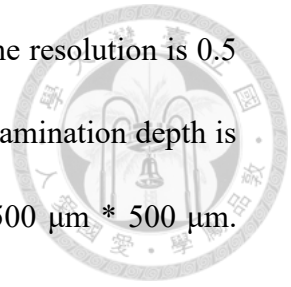


Fig. 5.3.3 Example of OCT-images presented in the study set. (A) Normal skin located on the arm, showing a narrow, hyperreflective band corresponding to an entry signal (thick arrow). The epidermis is seen as a homogenous well-demarcated darker layer (marked by \*). The dermis is seen as a lighter layer (marked by \*\*) and the DEJ is seen as a clear transition between the layers (thin arrow). (C) AK lesion located on the scalp, showing thickening of the epidermis (marked by \*) and purple streaks in the upper epidermis due to hyperkeratosis (thick arrow). The DEJ is disrupted beneath the thickened epidermis (marked by \*\*). Copyright: J. Olsen, L. Themstrup, N. De Carvalho, M. Mogensen, G. Pellacani, G. B. E. Jemec, "Diagnostic accuracy of optical coherence tomography in actinic keratosis and basal cell carcinoma", *Photodiagnosis and Photodynamic Therapy*, 2016, 16 (44-49) with permission from Elsevier.

The result is that skilled OCT observers were able to diagnose AK lesions with a sensitivity of 59% to 97% (average 76%) and a specificity of 52% to 83% (average 68%). Skilled observers with at least one year of OCT-experience showed an overall higher diagnostic accuracy compared to inexperienced observers. The conclusion is that diagnostic accuracy of differentiating AK from healthy skin has improved obviously than earlier OCT technology. But in comparison with H&E, the features of AK in OCT to distinguish normal from AK are the thickness of epidermis and the location of dermis-epidermis junction, which is imprecise to compare AKs from normal skin without the morphology of basal cells. Moreover, OCT did not indicate the grade of AK and they also did not show treatment assessment of AK by OCT.

---

For RCM, the typical system is Vivascope 1000/1500 where the resolution is 0.5 to 1.0  $\mu\text{m}$  in the lateral and 3 to 5  $\mu\text{m}$  in the axial dimension. An examination depth is 350  $\mu\text{m}$ , which corresponds to the papillary dermis. The FOV is 500  $\mu\text{m}$  \* 500  $\mu\text{m}$ .



Their images are shown in Fig. 5.3.4 to Fig. 5.3.7.<sup>[13][14]</sup>

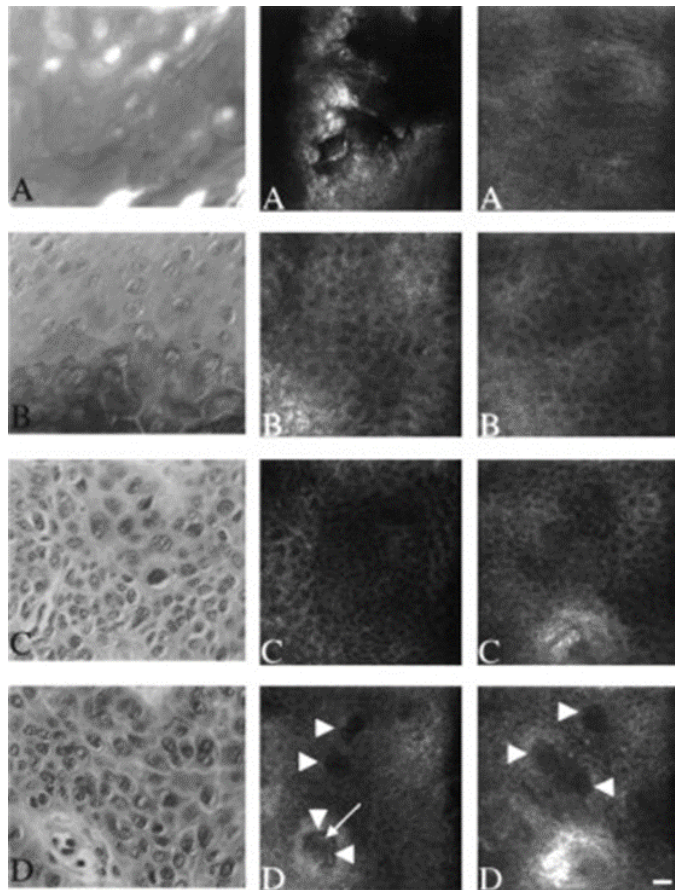


Fig. 5.3.4 Horizontal sections from depths in epidermis. Left column is conventional histopathology of AK, center is RCM of AK, and right column is RCM of adjacent normal skin. (A) Stratum corneum. (B) Stratum granulosum. (C) Stratum spinosum. (D) Stratum basale. Copyright: D. Aghassi, R. Anderson, S. González, “Confocal laser microscopic imaging of actinic keratoses *in vivo*: A preliminary report.” *Journal of the American Academy of Dermatology*, 2000, 43 (42-48) with permission from Elsevier.

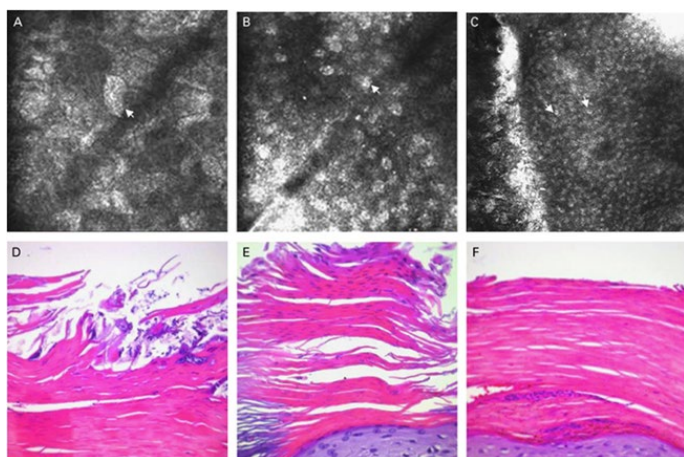


Fig. 5.3.5 The stratum corneum (A–C) RCM images; (D–F) representative histologic images. Copyright: M. Mlrich, A. Maltusch, F.-D. Rius, J. Röwert-Huber, S. González, W. Sterry, E. Stockfleth, S. Astner, “Clinical applicability of in vivo reflectance confocal microscopy for the diagnosis of actinic keratoses.” *Dermatologic Surgery*, 2008, 34:5 (610-619) with permission from Elsevier.

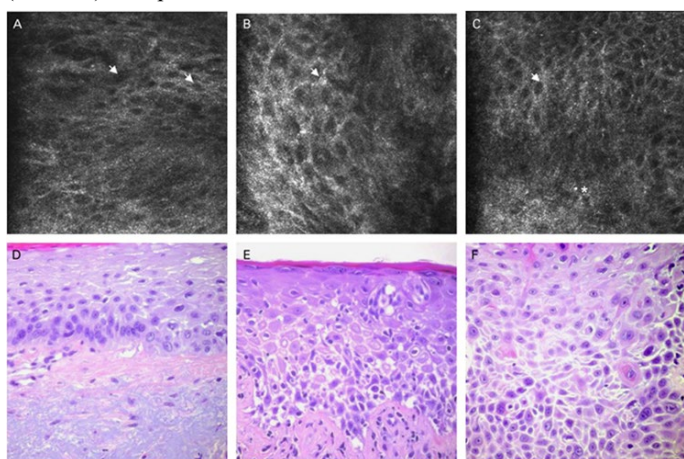


Fig. 5.3.6 Stratum granulosum and stratum spinosum (A–C) RCM images; (D–F) representative histologic images. Copyright: M. Mlrich, A. Maltusch, F.-D. Rius, J. Röwert-Huber, S. González, W. Sterry, E. Stockfleth, S. Astner, “Clinical applicability of in vivo reflectance confocal microscopy for the diagnosis of actinic keratoses.” *Dermatologic Surgery*, 2008, 34:5 (610-619) with permission from Elsevier.

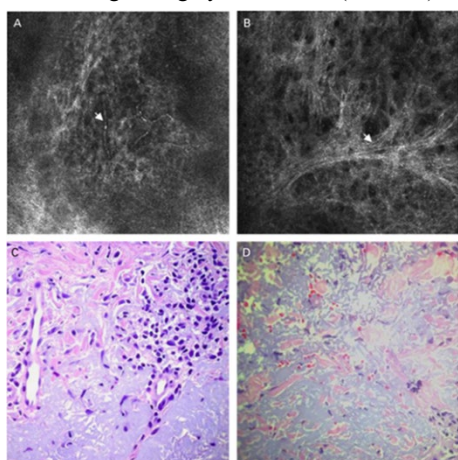


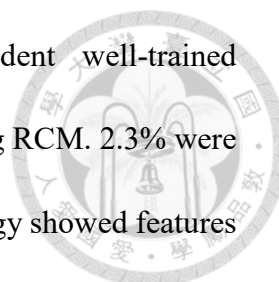
Fig. 5.3.7 Dermis (A, B) RCM images; (C, D) representative histologic images. Copyright: M. Mlrich, A. Maltusch, F.-D. Rius, J. Röwert-Huber, S. González, W. Sterry, E. Stockfleth, S. Astner, “Clinical applicability of in vivo reflectance confocal microscopy for the diagnosis of actinic keratoses.” *Dermatologic Surgery*, 2008, 34:5 (610-619)

---

with permission from Elsevier.

In Fig. 5.3.4, upon evaluation of the stratum corneum, superficial disruption can be found but the parakeratosis is not easily identified. The morphology of the stratum basale is not easily recognized in comparison with the morphology of the stratum spinosum in Fig. 5.3.4 C and D. In Fig. 5.3.5 to Fig. 5.3.7, they did not show the images in the stratum basale in this paper<sup>[14]</sup>. However, the morphology of the stratum basale is the most important for AK diagnosis. Because pathological changes of the mild AK are only in the stratum basale. In the fact, spinosum cells are bigger than basal cells. The morphology of the stratum spinosum of RCM is more legible than the morphology of the stratum basale of RCM due to the resolution. So, RCM prefers to show the images of the stratum spinosum instead of the images of the stratum basale. This is not appropriate for diagnosis of doctors. Moreover, in Fig. 5.3.4 the images are in low signal to background ratio in comparison with HGM images.<sup>[50]</sup> Low signal to background ratio makes the morphology of cells hard to be recognized. In Fig. 5.3.7, they declared that RCM could distinguish the solar elastosis because the signal intensity would be enhanced by elastin materials which is shown in the bright area of the dermis (arrows in Fig. 5.3.7 A and B) in RCM images. But collagen fibers also can cause the bright area of the dermis (Situations are the same as in arrows in Fig. 5.3.7 A and B.). RCM cannot distinguish elastin fibers from collagen fibers. So, it is unpersuasive that RCM can distinguish solar elastosis. The same as OCT, the main work of RCM was also calculating the sensitivity of AK by kappa analysis. Although RCM could show the morphology of all epidermis, they did not show the comparison results of H&E and RCM images in each diagnosis standard. With a total of 44 AKs included in the final

analysis and following blinded evaluation by two independent well-trained investigators, 97.7% of all skin samples were identified as AK using RCM. 2.3% were incorrectly identified as normal skin by RCM, while routine histology showed features consistent with AK (RCM and H&E in each patient). While if the observers were not trained, the result was 20 percent drop to 75.6% of all skin samples to be identified as AK correctly. Moreover, RCM did not indicate the grade of AK and they also did not show treatment assessment of AK. We list the summary of HGM, RCM and OCT in Table 5.3.8. Details of diagnosis criterions of HGM, RCM and OCT are shown in Table 5.3.9.



	OCT <sup>[12]</sup>	RCM <sup>[13][14]</sup>	HGM (This work)
Lateral resolution	7.5 μm to 10 μm	0.5 to 1.0 μm	395 nm
Penetration depth	2 mm	350 μm	250 μm
FOV	6 X 6 mm	500 X 500 μm	235 μm X 235 μm
Morphology	Rough	Low grade	Legible
Signal to background ratio	Low	Low	High
Number of identified diagnosis criterions	1	9	9
Wavelength	1320 nm	800 to 900 nm	1260 nm
Treatment assessment	No	No	Yes
AK grade	No	No	Yes
Sensitivity of AKs (untrained / well-trained)	68% / 76%	75.6% / 97.7%	100% / 100%

Table 5.3.8 The comparison of OCT, RCM and HGM.

		OCT <sup>[12]</sup>	RCM <sup>[13][14]</sup>	HGM (This work)
Stratum corneum	Parakeratosis	-	+	+
	Hyperkeratosis	+	+	+
Stratum spinosum	Irregular acanthosis	-	+	+
	Abnormal architecture	-	+	+
	Pleomorphisms of cells and nuclei	-	+	+
Stratum basale	Crowding of keratinocytes	-	+	+
	Abnormal architecture	-	+	+
	Pleomorphisms of abnormal cells and nuclei	-	+	+
dermis	solar elastosis	-	+	+

Table 5.3.9 Diagnosis criterions of HGM, RCM and OCT. “+” represents that this feature can be recognized. “-”

---

represents that this feature is uncertain to recognize.

In our work, the resolution of images is better than RCM and way much better than OCT. FOV is less than them and penetration depth is lowest on 250  $\mu\text{m}$ , due to the limitation on the working distance. But 250  $\mu\text{m}$  already corresponds to the papillary dermis and it can satisfy almost cases of AK diagnosis (especially AK I and AK II) if the epidermis is not thickened significantly. However, for AK III it suggests better penetration depth. Because the thickness of epidermis is thickened significantly. In AK patient 00, the thickness of epidermis was  $\sim 250 \mu\text{m}$ . Moreover, our resolution and signal to background ratio are better than the RCM and OCT and it means better morphology. In Table 5.3.9, it shows the details of diagnosis criterions of HGM, RCM and OCT. OCT only distinguishes AK from normal skin by the thickness of epidermis and it is completely unpersuasive for the pathologist. HGM and RCM can show the morphology of all diagnosis standards in epidermis. But the morphology of HGM is more legible than the morphology of RCM.

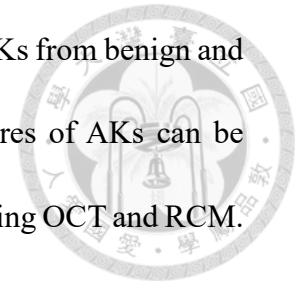
To show the HGM morphology of different layers of AKs, we collected 5 patients including 1 *ex vivo* and 4 *in vivo* shown in chapter 5.2. Moreover, we also tracked 1 patient to show the treatment assessment of AK.

In our study, the main work is the comparison of morphology of HGM and H&E images especially in the stratum basale which is the most important standard for diagnosis. We also tracked the location of multiple AK lesions for patients and showed the treatment assessment.

From the above, the diagnosis and treatment of AK are important because these lesions represent precursors to SCC that can be cured before malignant degeneration.

---

Real-time HGM offers a non-invasive opportunity to differentiate AKs from benign and malignant lesions without biopsy. By this study, pathologic features of AKs can be recognized legibly by HGM compared to existing technology including OCT and RCM.



Moreover, HGM can provide some unique findings.

1. HGM provides more legible morphology due to resolution and the much-improved signal to background ratio.
2. In the dermis, HGM can distinguish solar elastosis accurately by quantified signal intensity.
3. Especially, HGM can find dendritic structures in the stratum basale without specific staining.

Unfortunately, depth of penetration imposes a limitation in this HGM system in the diagnosis of AKs (AK III) especially for hyperkeratotic lesions. But generally speaking, the wavelength of laser source of RCM is 800 to 900 nm. The wavelength of the laser source of OCT is 1320 nm and the wavelength of the laser source of HGM is 1260 nm. So, considering the light diffusion and absorption of skin, the penetration depth of HGM is the best. In practice, two reasons are obvious. One is the limitation by working distance of our adopted objective (UAPON340/40X/NA=1.15, Olympus, Tokyo, Japan). Because our HGM system needs the good morphology (resolution) which means high NA. So, it is hard to be long in work distance for objective with high NA in the meanwhile. The other reason is that AKs are mostly surmounted by significant hyperkeratosis (AK III), which impedes the penetration of laser beam into the epidermis.

---

In addition, another limitation is that those AK patients are usually too old to keep still. So, the images are easy to be fuzzy by shaking of patients. More seriously, some layers were disappeared in image stacks due to the violent shaking in our clinical trials. In this study, the 5 patients were all over 70 years old. Therefore, we developed the movable system for clinical trials to reduce the impact of shaking by patients.

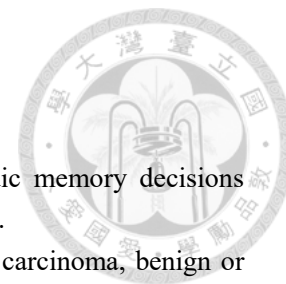
Most people get more than one AK lesion, and patients who have multiple AKs continue to get new AKs for life. Clinical diagnosis and treatment follow-up for multiple AKs mainly depend on visual inspection and direct counting of all visible lesions. Problems in the direct counting approach may reside in difficulty in dealing with small or almost contiguous lesions. In addition, it is difficult to track the same AK lesion according to the location on the face and its size progression if there are multiple lesions scattered on the whole face. With our 3D facial images system, HGM is potential to track the multiple locations of AKs and it can record all locational information accurately. We have tested one patient to show the tracking of an AK lesion.

Despite these limitations, our case study indicates that HGM may become an alternative to biopsy in the diagnosis of AKs and also help doctors to improve treatment efficiency.



---

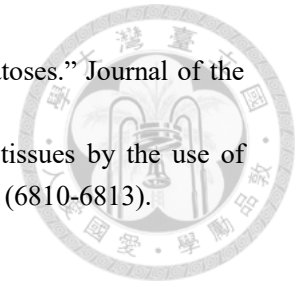
## REFERENCES



- [1] K. Duncan, A. Sadanand, L. Davachi, "Memory's penumbra: episodic memory decisions induce lingering mnemonic biases." *Science*, 2012, 337:6093 (485-487).
- [2] H. Robert, M. Lawrence, "Solar keratosis: an evolving squamous cell carcinoma, benign or malignant?" *Dermatologic Surgery*, 1995, 21:2 (184).
- [3] M.-H. Gold, M.-S. Nestor, "Current treatments of actinic keratosis." *Journal of Drugs in Dermatology*, 2006, 5:2 (17-25).
- [4] E.-E. Uhlenhake, "Optimal treatment of actinic keratoses." *Clinical Interventions in Aging*, 2013, 8 (29-35).
- [5] R. Marks, G. Renni, T.-S. Selwood, "Malignant transformation of solar keratoses to squamous cell carcinoma." *Lancet*, 1988, 331:8589 (795-797).
- [6] M.-J. Dodson, J.-D. Spain, J.-E. Hewett, "Malignant transformation of actinic keratosis and the controversy over treatment: a patient-oriented perspective." *Archives of Dermatology*, 1991, 127:7 (1029-1031).
- [7] F. Aaron, M. Ellen, "The kinetics of skin cancer: progression of actinic keratosis to squamous cell carcinoma." *Dermatologic Surgery*, 2007, 33:9 (1099-1101).
- [8] W. Fu, C.-J. Cockerell, "The actinic (solar) keratosis: a 21st-century perspective." *Archives of Dermatology*, 2003, 139:1 (66-70).
- [9] K.-O. Duncan, J.-K. Geisse, D.-J. Leffell, "Epithelial precancerous lesions." 2012, (261-492).
- [10] Y.-H. Liao, K.-H. Chen, M.-P. Tseng, C.-C. Sun, "Pattern of skin diseases in a geriatric patient group in Taiwan: A 7-year survey from the outpatient clinic of a university medical center." *Dermatology*, 2001, 203:4 (308-313).
- [11] L. Themstrup, G. Pellacani, J. Welzel, J. Holmes, G.-B.-E. Jemec, M. Ulrich, "In vivo microvascular imaging of cutaneous actinic keratosis, Bowen's disease and squamous cell carcinoma using dynamic optical coherence tomography." *The Journal of the European Academy of Dermatology and Venereology*, 2017, 31:10 (1655-1662).
- [12] J. Olsen, L. Themstrup, N. Carvalho, M. Mogensen, G. Pellacani, G.-B.-E. Jemec, "Diagnostic accuracy of optical coherence tomography in actinic keratosis and basal cell carcinoma." *Photodiagnosis and Photodynamic Therapy*, 2016, 16 (44-49).
- [13] M. Ulrich, A. Maltusch, J. Röwert-Huber, S. González, W. Sterry, E. Stockfleth, S. Astner, "Actinic keratoses: non-invasive diagnosis for field cancerization." *The British Journal of Dermatology*, 2007, 156:3 (13-17).
- [14] M. Ulrich, A. Maltusch, F.-D. Rius, J. Röwert-Huber, S. González, W. Sterry, E. Stockfleth, S. Astner, "Clinical applicability of in vivo reflectance confocal microscopy for the diagnosis of actinic keratoses." *Dermatologic Surgery*, 2008, 34:5 (610-619).
- [15] M.-R. Tsai, S.-Y. Chen, D.-B. Shieh, P.-J. Lou, C.-K. Sun, "In vivo optical virtual biopsy of human oral mucosa with harmonic generation microscopy." *Biomedical Optics Express*, 2011, 2:8 (2317-2328).
- [16] M.-R. Tsai, D.-B. Shieh, P.-J. Lou, C.-F. Lin, C.-K. Sun, "Characterization of oral squamous cell carcinoma based on higher-harmonic generation microscope." *Journal of Biophotonics*, 2012, 5:5-6 (415-424).
- [17] M.-R. Tsai, Y.-H. Cheng, J.-S. Chen, Y.-S. Sheen, Y.-H. Liao, C.-K. Sun, "Differential

- diagnosis of nonmelanoma pigmented skin lesions based on harmonic generation microscopy.” *Journal of Biomedical Optics*, 2014, 19:3 (036001).
- [18] M.-R. Tsai, C.-Y. Lin, Y.-H. Liao, C.-K. Sun, “Applying tattoo dye as a third-harmonic generation contrast agent for in vivo optical virtual biopsy of human skin.” *Journal of Biomedical Optics*, 2013, 18:2 (026012).
- [19] G. J. Brakenhoff, J. Squier, T. Norris, A. C. Bliton, M. H. Wade, B. Athey, “Real-time two-photon confocal microscopy using a femtosecond, amplified Ti:sapphire system.” *Journal of Microscopy*, 1996, 181:3 (253-259).
- [20] Y.-C. Guo, P.-P. Ho, H. Savage, D. Harris, P. Sacks, S. Schantz, L. Feng, N. Zhadin, R. R. Alfano, “Second-harmonic tomography of tissues.” *Optics Letters*, 1997, 22:17, (1323-1325).
- [21] C. G. Omar, A. C. Millard, C. B. Schaffer, J. A. Au, P.-S. Tsai, J. A. Squier, D. Kleinfeld, “Spectroscopy of third-harmonic generation: evidence for resonances in model compounds and ligated hemoglobin.” *Journal of the Optical Society of America B*, 2006, 23:5 (932-950).
- [22] J. Squier, “High resolution nonlinear microscopy: A review of sources and methods for achieving optimal imaging.” *Review of Scientific Instruments*, 2001, 72:7 (2855-2867).
- [23] S.-Y. Chen, Y.-H. Wu, S.-K. Sun, “In vivo harmonic generation biopsy of human skin.” *Journal of Biomedical Optics*, 2009, 14:6 (060505).
- [24] H.-Y. Liao, S.-Y. Chen, S.-Y. Chou, P.-H. Wang, M.-R. Tsai, C.-K. Sun, “Determination of chronological aging parameters in epidermal keratinocytes by in vivo harmonic generation microscopy.” *Biomed Optics Express*, 2013, 4:1 (77-88).
- [25] Y.-H. Liao, W.-C. Kuo, S.-Y. Chou, C.-S. Tsai, G.-L. Lin, M.-R. Tsai, Y.-T. Shih, G.-G. Lee, C.-K. Sun, “Quantitative analysis of intrinsic skin aging in dermal papillae by in vivo harmonic generation microscopy.” *Biomed Optics Express*, 2014, 5:9 (3266-3279).
- [26] S.-Y. Chen, S.-U. Chen, H.-Y. Wu, W.-J. Lee, Y.-H. Liao, C.-K. Sun, “In vivo virtual biopsy of human skin by using noninvasive higher harmonic generation microscopy.” *IEEE Journal of Selected Topics in Quantum Electronics*, 2010, 16:3 (478-492).
- [27] C. J. Cockerell, “Histopathology of incipient intraepidermal squamous cell carcinoma.” *The American Journal of Dermatopathology*, 2000, 42:1 (11-17).
- [28] <https://commons.wikimedia.org/wiki/File:Skinlayers.png>
- [29] <https://www.skincancer.org/skin-cancer-information/actinic-keratosis>
- [30] G. M. James, M. Jeffery, “Looking bill and mark principles of dermatology.” 2006 4th edition (40).
- [31] R. E. Jones, “Questions to the editorial board and other authorities.” *The American Journal of Dermatopathology*, 1984, 4:1 (91-95).
- [32] D. Weedon, “Weedon's Skin Pathology” 2010 3rd edition (56-57).
- [33] A. Michele, D. Mittelbronn, D. L. Mullins, R.-C. A. Francisco, F. P. Flowers, “Frequency of pre - existing actinic keratosis in cutaneous squamous cell carcinoma.” *International Journal of Dermatology*, 1998, 37:9 (677-681).
- [34] R. A. Schwartz, “The actinic keratosis: a perspective and update.” *Dermatologic Surgery*, 1997, 23:11 (1009-1019).
- [35] L. Julien, C. Chen, G. Goldenberg, “Actinic keratosis as a marker of field cancerization in excision specimens of cutaneous malignancies.” *Cutis*, 2016, 97:6 (415-420).
- [36] [https://commons.wikimedia.org/wiki/File:Bowenoid\\_actinic\\_keratosis\\_-\\_high\\_mag.jpg](https://commons.wikimedia.org/wiki/File:Bowenoid_actinic_keratosis_-_high_mag.jpg)
- [37] T. Day, S. M. Holland, J. P. Scurry, “Normal vulvar histology: variation by site.” *Journal of*

- 
- Lower Genital Tract Disease, 2016, 20:1 (64-69).
- [38] R. R. Lubritz, S. A. Smolewski, "Cryosurgery cure rate of actinic keratoses." *Journal of the American Academy of Dermatology*, 1982, 7:5 (631-632).
- [39] Y.-C. Guo, R.-R. Alfano, "Optical harmonic generation from animal tissues by the use of picosecond and femtosecond laser pulses." *Applied Optics*, 1996, 35:34 (6810-6813).
- [40] "The 10 golden rules of laser safety" 2007, University of Nottingham.
- [41] "Laser safety manual" 1998, California Institute of Technology.
- [42] S.-Y. Chen, H.-Y. Wu, C.-K. Sun, "In vivo harmonic generation biopsy of human skin." *Journal of Biomed Optics* 2009, 14:6 (060505).
- [43] A. Böhling, S. Bielfeldt, A. Himmelmann, M. Keskin, K. P. Wilhelm, "Comparison of the stratum corneum thickness measured in vivo with confocal Raman spectroscopy and confocal reflectance microscopy." *Skin Research and Technology*, 2014, 20:1 (50-57).
- [44] Y.-X. Zhen, S. Takaki, H. Tagami, "Number of cell layers of the stratum corneum in normal skin –relationship to the anatomical location on the body, age, sex and physical parameters." *Archives for Dermatological Research*, 1999, 291:10 (555-559).
- [45] [https://www.histology.leeds.ac.uk/skin/epidermis\\_layers.php](https://www.histology.leeds.ac.uk/skin/epidermis_layers.php)
- [46] C.-H. Yu, C.-K. Sun, "In vivo and ex vivo imaging of intra-tissue elastic fibers using third-harmonic-generation microscopy." *Optics Express*, 2007, 15:18 (11167-11177).
- [47] L. Schmitz, P. Kahl, M. Majores, E. Bierhoff, E. Stockfleth, T. Dirschka, "Actinic keratosis: correlation between clinical and histological classification systems." *The Journal of the European Academy of Dermatology*, 2016, 30:8 (1303-1307).
- [48] J. V. Schmitt, H. A. Miot, "Actinic keratosis: a clinical and epidemiological revision." *Brazilian Society of Dermatology*, 2012, 87:3 (425-434).
- [49] W.-H. Weng, C.-K. Sun, "Differentiating intratumoral melanocytes from Langerhans cells in nonmelanocytic pigmented skin tumors in vivo by label-free third harmonic generation microscopy." *Journal of Biomedical Optics*, 2016, 21:7 (076009).
- [50] Y.-F. Qi, C. Xu, "Multi-color background-free coherent antistokes Raman scattering microscopy using a time-lens source." *Optics Express*, 2018, 26:26 (34474-34483).



# COPYRIGHT



1. Fig. 2.2.1 is modified by Serephine in 16 November 2006. These images are in the public domain. The licensing is shown in website:

<https://commons.wikimedia.org/wiki/File:Skinlayers.png>

Licensing [edit]



I, the copyright holder of this work, release this work into the **public domain**. This applies worldwide.  
In some countries this may not be legally possible; if so:  
I grant anyone the right to use this work **for any purpose**, without any conditions, unless such conditions are required by law.

2. Fig. 2.3.3.1(a) is modified in Feb 2010 by Nephron. It is own work in Wikimedia commons. The licensing is from website:

[https://commons.wikimedia.org/wiki/File:Bowenoid\\_actinic\\_keratosi\\_s\\_high\\_mag.jpg](https://commons.wikimedia.org/wiki/File:Bowenoid_actinic_keratosi_s_high_mag.jpg)

Licensing [edit]

I, the copyright holder of this work, hereby publish it under the following licenses:

This file is licensed under the Creative Commons Attribution-Share Alike 3.0 Unported license.

You are free:

- to **share** – to copy, distribute and transmit the work
- to **remix** – to adapt the work

Under the following conditions:

- **attribution** – You must give appropriate credit, provide a link to the license, and indicate if changes were made. You may do so in any reasonable manner, but not in any way that suggests the licensor endorses you or your use.
- **share alike** – If you alter, transform, or build upon this work, you may distribute the resulting work only under the same or similar license to this one.

3. The license of Fig. 2.3.3.1(b):

2019/4/25 RightsLink Printable License

**WOLTERS KLUWER HEALTH, INC. LICENSE TERMS AND CONDITIONS** Apr 24, 2019

---

This Agreement between Mr. Pan Yi ("You") and Wolters Kluwer Health, Inc. ("Wolters Kluwer Health, Inc.") consists of your license details and the terms and conditions provided by Wolters Kluwer Health, Inc. and Copyright Clearance Center.

License Number	4575500704407
License date	Apr 24, 2019
Licensed Content Publisher	Wolters Kluwer Health, Inc.
Licensed Content Publication	Journal of Lower Genital Tract Disease
Licensed Content Title	Normal Vulvar Histology: Variation by Site
Licensed Content Author	Tania Day, Seán Holland, and James Scurry
Licensed Content Date	Jan 1, 2016
Licensed Content Volume	20
Licensed Content Issue	1
Type of Use	Dissertation/Thesis
Requestor type	Individual
STM publisher name	
Portion	Figures/table/illustration
Number of figures/tables/illustrations	2
Figures/tables/illustrations used	Fig. 2
Author of this Wolters Kluwer article	No
Title of your thesis / dissertation	Application of a Three-dimensional Tracking System with Harmonic Generation Microscope for Diagnosing Multiple Actinic Keratosis
Expected completion date	Apr 2019
Estimated size(pages)	1
Requestor Location	Mr. Pan Yi Taiwan
	Taipei, 321100 China Attn: Mr. Pan Yi
Total	0.00 USD
Terms and Conditions	

4. The license of Fig. 5.3.3:

**ELSEVIER LICENSE  
TERMS AND CONDITIONS**

Apr 22, 2019

This Agreement between Mr. Pan Yi ("You") and Elsevier ("Elsevier") consists of your license details and the terms and conditions provided by Elsevier and Copyright Clearance Center.

License Number	4574331492010
License date	Apr 22, 2019
Licensed Content Publisher	Elsevier
Licensed Content Publication	Journal of the American Academy of Dermatology
Licensed Content Title	Confocal laser microscopic imaging of actinic keratoses in vivo: A preliminary report
Licensed Content Author	David Aghassi, R.Rox Anderson, Salvador González
Licensed Content Date	Jul 1, 2000
Licensed Content Volume	43
Licensed Content Issue	1
Licensed Content Pages	7
Start Page	42
End Page	48
Type of Use	reuse in a thesis/dissertation
Portion	figures/tables/illustrations
Number of figures/tables/illustrations	2
Format	both print and electronic
Are you the author of this Elsevier article?	No
Will you be translating?	No
Order reference number	00752584
Original figure numbers	Fig. 2
Title of your thesis/dissertation	Application of a Three-dimensional Tracking System with Harmonic Generation Microscope for Diagnosing Multiple Actinic Keratosis
Expected completion date	Apr 2019
Estimated size (number of pages)	1
Requestor Location	Mr. Pan Yi Taiwan
	Taipei, 321100 China Attn: Mr. Pan Yi
Publisher Tax ID	GB 494 6272 12
Total	0.00 USD
Terms and Conditions	



5. The license of Fig. 5.3.4:

**ELSEVIER LICENSE  
TERMS AND CONDITIONS**

Apr 22, 2019

This Agreement between Mr. Pan Yi ("You") and Elsevier ("Elsevier") consists of your license details and the terms and conditions provided by Elsevier and Copyright Clearance Center.

License Number	4574340294341
License date	Apr 22, 2019
Licensed Content Publisher	Elsevier
Licensed Content Publication	Photodiagnosis and Photodynamic Therapy
Licensed Content Title	Diagnostic accuracy of optical coherence tomography in actinic keratosis and basal cell carcinoma
Licensed Content Author	J. Olsen, L. Themstrup, N. De Carvalho, M. Mogensen, G. Pellacani, G.B.E Jemec
Licensed Content Date	Dec 1, 2016
Licensed Content Volume	16
Licensed Content Issue	n/a
Licensed Content Pages	6
Start Page	44
End Page	49
Type of Use	reuse in a thesis/dissertation
Intended publisher of new work	other
Portion	figures/tables/illustrations
Number of figures/tables/illustrations	3
Format	both print and electronic
Are you the author of this Elsevier article?	No
Will you be translating?	No
Order reference number	00752584
Original figure numbers	Fig.3
Title of your thesis/dissertation	Application of a Three-dimensional Tracking System with Harmonic Generation Microscope for Diagnosing Multiple Actinic Keratosis
Expected completion date	Apr 2019
Estimated size (number of pages)	1
Requestor Location	Mr. Pan Yi Taiwan  Taipei, 321100 China Attn: Mr. Pan Yi
Publisher Tax ID	GB 494 6272 12
Total	0.00 USD

6. The license of Fig. 5.3.5, Fig. 5.3.6 and Fig. 5.3.7:

**WOLTERS KLUWER HEALTH, INC. ORDER DETAILS**

Apr 22, 2019

Order Number	501480225
Order date	Apr 22, 2019
Licensed Content Publisher	Wolters Kluwer Health, Inc.
Licensed Content Publication	Dermatologic Surgery
Licensed Content Title	Clinical Applicability of in vivo Reflectance Confocal Microscopy for the Diagnosis of Actinic Keratoses
Licensed Content Author	MARTINA ULRICH, ADRIENNE MALTUSCH, FRANCISCA RIUS-DIAZ, et al
Licensed Content Date	May 1, 2008
Licensed Content Volume	34
Licensed Content Issue	5
Type of Use	Dissertation/Thesis
Requestor type	Individual
Portion	Figures/table/illustration
Number of figures/tables/illustrations	3
Figures/tables/illustrations used	Fig.1, Fig.2 , Fig.3
Author of this Wolters Kluwer article	No
Order reference number	00752587
Title of your thesis / dissertation	Application of a Three-dimensional Tracking System with Harmonic Generation Microscope for Diagnosing Multiple Actinic Keratosis
Expected completion date	Apr 2019
Estimated size(pages)	1
Requestor Location	Mr. Pan Yi Taiwan  Taipei, 321100 China Attn: Mr. Pan Yi